**Exploration of 3D Phage-Based Biomolecular Filter for Filtration of Foodborne Pathogens in Large Volume of Liquid Streams**

By

Songtao Du

A dissertation submitted to the Graduate Faculty of
Auburn University
in partial fulfillment of the
requirements for the Degree of Doctor of Philosophy

Auburn, Alabama
August 8, 2020

Keywords: 3D filter, ME filter elements,
E2 phage, Capture rate, *Salmonella typhimurium*, Turbulence



Approved by

Dr. Pengyu Chen, Assistant Professor, Material Engineering
Dr. Zhongyang Cheng, Professor, Material Engineering
Dr. Dong-Joo Kim, Professor, Material Engineering
Dr. Wei Zhan, Associate Professor, Department of Chemistry and Biochemistry
Dr. Tung-Shi Huang, Professor, Department of Poultry Science

Abstract

A three-dimensional phage-based biomolecular filter (3D filter) was designed and developed to capture, concentrate, and isolate foodborne pathogens from large volume of liquid streams with high throughput, such as liquid food and water used to process foods. The 3D filter consisted of E2 phage-immobilized magnetoelastic (ME) filter elements, a controlled magnetic field, and a 3D filter pipe system. Due to the high selectivity and specific binding affinity, the filamentous E2 phage was utilized to capture *Salmonella typhimurium* pathogens in large volume of liquid streams with high throughput. The ME filter elements were aligned in the 3D filter pipe system by the controlled magnetic field. The target pathogens can be captured by the ME filter elements in the 3D filter pipe system, while the debris and non-target pathogens would pass through the 3D filter system with the liquid steams. Therefore, the 3D phage-based biomolecular filter was developed for an anti-clogging specific filtration with a high throughput. In this dissertation, two generations of the 3D filter (3D filter 1.0 &2.0) were developed and tested.

The 3D filter 1.0 system was formed by ME filter elements, supporting frames with solenoid coils, and a 3D filter pipe system. The ME filter elements were aligned on the supporting frames by electromagnetic field produced from the solenoid coils. The soft magnetic material of the supporting frames was selected from the commercial market, and the structure of the supporting frames was designed and fabricated. The magnetic field was simulated and measured by Ansys Workbench and Gaussmeter. For foodborne pathogens capturing experiments, the effect of temperature variation on the E2 phage and the *Salmonella typhimurium* suspensions was firstly tested in the 3D filter 1.0 pipe system, followed by *Salmonella typhimurium* capturing experiments. The increased capture rate

was illustrated with the increased number of filter layers. However, the filtration of *Salmonella* pathogens was not realized due to the low density of aligned ME filter elements and the low capture rate.

Because of the low capture rate, the filtering capability of ME filter elements was explored by 2D filter experiment, followed by the development of 3D filter 2.0 system without the supporting frames. For the 3D filter 2.0 system, a pair of permanent magnetic plates was used to align the ME filter elements in the 3D filter 2.0 pipe system instead of the solenoid coils. The development of the 3D filter 2.0 was divided into three stages, including the initial 3D filter 2.0, the large-scale 3D filter 2.0, and the multipipe-3D filter 2.0. The filtration of *Salmonella* pathogens was demonstrated by the initial 3D filter 2.0. The anti-clogging characteristic and high throughput performance were demonstrated by the large-scale 3D filter 2.0, as well as the filtering performance of *Salmonella* pathogens with the increased number and the total surface area of ME filter elements. The turbulent flow condition of pathogen suspensions and the capture rate were also simulated and discussed in the stage of initial 3D filter 2.0 and the large-scale 3D filter 2.0. In the third stage, the multipipe-3D filter system with circulation flow of pathogen suspensions was used to explore the filtering performance with the increased volume of liquid streams. The interaction between the cyclic times for 90% capture rate and the volumes of pathogen suspensions was investigated by the multipipe-3D filter system with circulation, which could be a reference to design the multipipe-3D filter system for a specific volume of pathogen suspensions.

Acknowledgments

I would like to thank my advisor Dr. Bryan Chin and Dr. Pengyu Chen's persistent help and expert guidance during my research at Auburn University. The dissertation would not have been possible without Dr. Chin and Dr. Pengyu's wisdom, patience, and encouragement. I also thank all my committee members, Dr. Zhongyang Cheng, Dr. Dong-Joo Kim, Dr. Iryna Sorokulova, Dr. Wei Zhan, and Dr. Tung-shi Huang, for their sincere help and support. The special thanks also go to Dr, Zhongyang Cheng and Dr. Pengyu Chen, who have helped me to improve my scientific thought, research attitude, and the academic researching methods. I am also grateful to Charles Ellis and John Sellers, who has helped me with the coil and ME transducer's microfabrication and I-Hsuan Chen, who has shared a great deal of biological knowledge, writing skills, and provided all the biological samples.

I am thankful for all the support from Dr. Shin Horikawa, Dr. Yating Chai, Dr. Jin Dai, Dr. Howard C. Wikle, Dr. Jianping He, Steve Best, Steven Moore, Yuzhe Liu, Alana MacLachlan, Jiajia Hu, Feng'en Wang, Jianguo Xi, and Jun Chen. I especially would like to give thanks to Dr. Shin Horikawa, who has shared with me countless discussions and ideas and given me lots of help on experiments, and Steve Moore, who has helped me to order experimental supply and train equipment.

Last but not least, I have immense gratitude for my family's love and understanding, for my Auburn friends' support, and the encouragement from my friends' in China.

Table of Contents

List of Tables

List of Figures

List of Abbreviations

| | |
|---|---|
| AWG | American Wire Gauge |
| CDC | Centers for Disease Control and Prevention |
| DI Water | Filtered Deionized Water |
| DNA | Deoxyribonucleic Acid |
| DPM | Discrete Particle Mode |
| EIA | Enzyme Immunoassay |
| EIS | Electrochemical Impedance Spectroscopy |
| ELISA | Enzyme-Linked Immunosorbent Assay |
| ELFA | Enzyme-Linked Fluorescent Assay |
| FDA | Food and Drug Administration |
| FTIR | Raman and Fourier Transform Infrared |
| HRP | Horseradish Peroxidase |
| LAPS | Light Addressable Potentiometric Sensor |
| ME | Magnetoelastic |
| PAB | Potentiometric Alternating Biosensing |
| PCR | Polymerase Chain Reaction |
| PNA | Peptide Nucleic Acid |
| QCM | Quartz Crystal Microbalance |
| RNA | Ribonucleic Acid |
| RODS | Real-time Outbreak Disease Surveillance |
| SAW | Surface Acoustic Wave |
| SEM | Scanning Electron Microscopy |

| | |
|---|---|
| SERS | Surface-Enhanced Raman Scattering |
| SPR | Surface Plasmon Resonance |
| TBS | Tris Buffered Saline |
| USDA | U.S. Department of Agriculture |
| UV | Ultraviolet |
| WEDM | Wire cut Electrical Discharge Machine |
| WHO | World Health Organization |

Chapter 1

# 1. Introduction

## 1.1. Background

In the twenty-first century, biosafety, such as food safety and bioterrorism attack issue, has been listed in one part of the national security relating to society, economy, health, and environment. Food safety is the most direct key factor for human health, resulting from food contamination. Multi-states outbreaks of foodborne illnesses occur each year due to the infection of foodborne pathogens, such as *Salmonella, E. coli, and Listeria*. Moreover, the safety issue of genetically modified food is always a focused topic for the public and media. The emergence of agricultural biotechnology has created social and ethical contradictions. The widespread debate exists as to how the transgene technique can be used for planting products with high quality and high yield while protecting eco-system and human health. Consumers are mainly concerned about the long term human health effects of genetically modified food, such as antibiotic resistance, unnatural nutritional changes, and toxicity (Maghari and Ardekani 2011). Furthermore, the potential risk can exist in society when microorganisms are utilized by terrorists to make biological warfare or outbreaks of contagions. Therefore, biosafety plays a significant role in the stabilization of society. In the introduction, the foodborne illness challenge, bioterrorism attack issue, and the bio-surveillance system are mainly discussed.

### 1.1.1. Foodborne illness challenge and public health issue

Foodborne illness is a common, costly public health issue, not only in developing countries but also in developed counties (Zeynep Altintas 2018). Each year, roughly one in six Americans get sick, resulting in 128,000 hospitalizations and 3,000 deaths (CDC

2019b). The number of multi-state outbreaks increases gradually in twenty years from 1998 to 2015, as shown in Figure 1.1. Besides the health issue, the cost of foodborne illness is also enormous. The direct and indirect cost associated with foodborne illnesses was more than $15.6 billion per year in the report of the U.S. Department of Agriculture (USDA) in 2014 (Stephen Ostroff 2018). Another estimation from Ohio State University showed that at least $55.5 billion was cost by foodborne illnesses (Stephen Ostroff 2018). So far, more than 250 foodborne diseases have been identified by researchers (CDC 2019b). Most foodborne illnesses are caused by a variety of bacteria, viruses, and parasites. Based on statistical data, the distributions of the number of literatures about the detection of pathogens are displayed by the industry of application and micro-organism in Figure 1.2, respectively (Lazcka, Campo, and Muñoz, 2007).

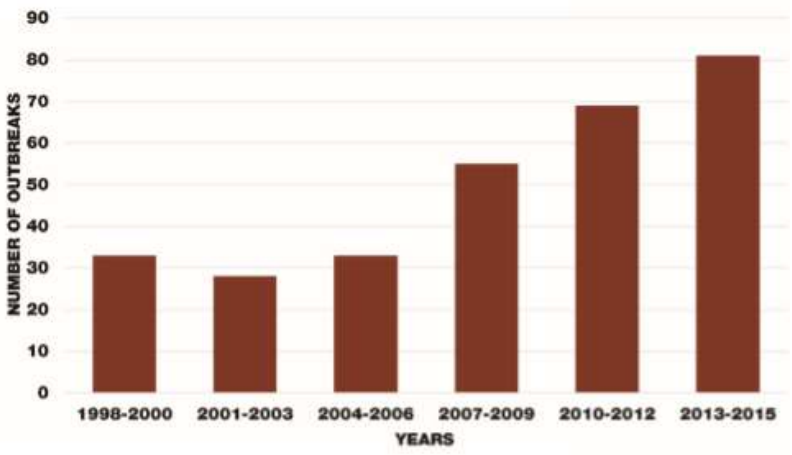


Figure 1. 1 Number of multi-states outbreaks from 1998 to 2015 (CDC 2018b).

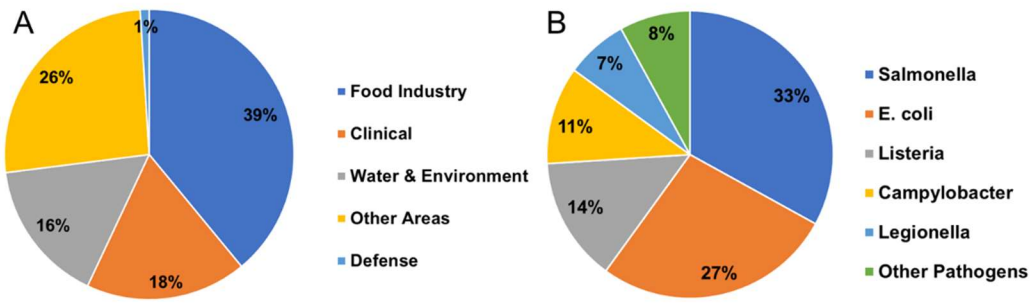

Figure 1. 2 Distribution of the number of literatures about pathogen detections by (A) industry of application and (B) microorganism.

*Salmonella* pathogen is one of the top five germs commonly causing foodborne illnesses. According to the CDC, *Salmonella* pathogen is estimated to annually cause more than one million foodborne illnesses in the United States, with 23,000 hospitalizations and 450 deaths (CDC 2019d). The symptoms of diarrhea, fever, and abdominal cramps are presented from most of the patients infected by *Salmonella* pathogens. In 2018, the multistate outbreak of Spring Pasta Salad from Hy-Vee, Inc exposed the possible contamination with *Salmonella Sandiego* and *Salmonella enterica* subspecies (CDC 2018c). One hundred and one people were infected with the outbreak strains from ten states (CDC 2018c). In 2019, the pre-cut melons supplied by the Caito Foods LLC facility in Indianapolis, Ind were recalled because of *Salmonella Carrau* contamination (CDC 2019c). A total of 137 infected people were reported from ten states.

Moreover, antibiotic resistance of foodborne pathogens is also a high-profile issue for food safety. Antibiotics can kill pathogens with a moderate dose. However, the drug-resistance of pathogens is increasing due to the overuse of antibiotics. Each year, at least two million people are infected by pathogens that are resistant to antibiotics, and at least 23,000 people die as a direct result of these infections (CDC 2019a).

### 1.1.2. Bioterrorism attack and national security

Besides food safety, bioterrorism attack is also a potential danger for the public in the world. The bioterrorism attack is the deliberate release of viruses, bacteria, or other germs to cause illnesses or death. These biological agents are relatively easy and inexpensive to get and spread through the air, water, and food (Wikipedia 2020b). They are often found

in nature, but they can also be made more harmful by increasing the ability of perniciousness to cause illness, death, spread, or resist medical treatment (Chai 2014). Thus far, thirty-five potential bioterrorism agents have been identified and classified into three categories by the CDC. The classification is based on the likelihood of the agent being used and the risk posed by each agent. The highest priority Category A agents include organisms that pose a risk to national security, since they can be easily disseminated or transmitted from person to person, resulting in high mortality rates and the potential for a major public health impact (CDC 2018a).

### 1.1.3. Bio-surveillance system

Bio-surveillance system is the science of real-time disease outbreak detection applied to both natural and human-made epidemics (Wikipedia 2020b). For the food safety issue, the most significant doubts are where the foodborne pathogens come and how to control and prevent more infections (Chai 2014). Thus, the bio-surveillance system should be operated to trace all food processing steps from farm to kitchen by videos, employees, locations, and reserved samples. By this system, each step can be checked to look for the appearance of foodborne pathogens when a foodborne illness outbreak is reported. And then, the etiology, source, and impact of foodborne pathogens are clarified by the epidemiological investigation (Chai 2014). For the well-understood pathogens, established methods of control and prevention can be used directly. For unknown pathogens, scientific research is applied to clarify and understand the infecting mechanism to develop therapies. Several organizations have built the surveillance system for the food safety issue, such as the CDC, USDA, and Food and Drug Administration (FDA). Outbreak conditions will be reported each time, including quantities of infecting people, states, the source of infection,

and how to prevent and control. Meanwhile, the experiences and information can also be collected and summarized for surveillance. The infection will be decreased, and the prevention will be successful in the continuous and highly effective circulation among epidemiological investigations, preventions, and surveillance in Figure 1.3. Since assembling information is time-consuming, the international coordination in the surveillance system is becoming more significant. The information can be shared rapidly and efficiently through networks. The networks in the world that cooperate with governments have been built by the World Health Organization (WHO) to share information, detect pathogens, and prevent outbreaks.

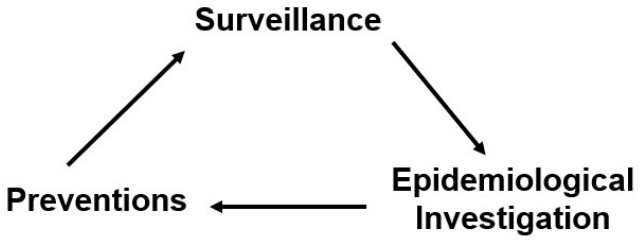


Figure 1. 3 Circulation of public health prevention and control.

The Bio-surveillance system is also significant for national security in an aspect of a bioterrorism attack. The first automated bioterrorism detection system, called real-time outbreak disease surveillance (RODS), was developed by the University of Pittsburgh's Center for biomedical informatics in 1990. RODS collected data from clinic, laboratory, company, and pharmacy to detect a possible bioterrorism event at an early time. Under the effort of RODS, the National Retail Data Monitor system was established to collect data from 20,000 retail locations nationwide in 2000 (Wikipedia 2020b). In 2002, the RODS laboratory was regarded as the standard to equip all fifty states with the bio-surveillance system (Wikipedia 2020b).

### 1.2. Objectives of research

Pathogen detection techniques play an essential role in detecting pathogen source and distinguishing pathogen category. Precaution and therapy also depend on detecting accuracy and time. Although traditional detection methods, such as culture and colony methods, immunology-based methods, and polymerase chain reaction (PCR), are sensitive and accurate, the complicated sample preparation is required, including sample collection, separation, and enrichment, which are time-consuming and professional, resulting in a delay in obtaining screening results. Due to the requirement of time-saving and easy operation, biosensing technologies were developed to rapidly and precisely detect pathogens from food surfaces and liquids. Biosensing technologies illustrate the characteristics of accuracy, low-cost, fast-response, stable, highly efficient, and user-friendly, which are successful for the small number of samples by random sampling. However, the total number of samples is limited for a large number of products, especially for liquid streams. Based on that, on-set and off-set filtration methods have been developed and widely applied for pathogen and toxins filtration from liquids, such as nanomagnetic beads or discs, carbon nanotube coated filter, and glass wool filter. However, porous pre-filter aid materials are needed to prevent a clogging issue, leading to multiple filtering steps needed, or some pathogen filtration methods are non-specific. Hence, it is of high priority and significant to develop an advanced method to specifically filter target-pathogens from large volumes of liquid streams with high throughput.

The impetus of this research is to develop an anti-clogging technology for filtration of foodborne pathogens from large volumes of liquid streams with high throughput. This

technology, named 3D phage-based biomolecular filter (3D filter), will ultimately benefit producers, food industry, and society with improved food safety.

To pursue the specific filtration of foodborne pathogens from large volumes of liquid streams with high throughput, the primary objective of this research is to design and develop the 3D phage-based biomolecular filter system to explore the anti-clogging characteristic, the capturing, and filtering performance by phage-immobilized ME filter elements in it. This research is focused mainly on the four steps:

1. Design, fabricate, and test the 1st version of the 3D phage-based biomolecular filter system with E2 phage-immobilized ME filter elements to capture *Salmonella typhimurium* pathogens from large volumes of pathogen suspensions.
2. Demonstrate the capturing and filtering capability of E2 phage-immobilized ME filter elements for *Salmonella typhimurium* pathogens from small volumes of pathogen suspensions by a 2D filter rocking system.
3. Design, fabricate, and initially test the 2nd version of 3D phage-based biomolecular filter with E2 phage-immobilized ME filter elements to capture and filter *Salmonella typhimurium* pathogens from the same pathogen suspensions in the second step.
4. Fabricate and explore the large-scale and multipipe 3D phage-based biomolecular filter in the 2nd version. The tests include anti-clogging characteristic, high throughput performance, capturing, and filtering performance for the large-scale 3D filter and filtering performance for the multipipe 3D filter.

### 1.3. Dissertation organization

In this chapter, the biosafety issues, the significance of bio-surveillance, and the objective of this research are introduced. The rest of the presentation is organized as follows:

Chapter 2 briefly introduces bio-probes used in laboratory research for pathogen detection and describes traditional detection methods and biosensing detection technologies in laboratories and commercial markets.

Chapter 3 describes theory, fabricating methods of ME transducer and filamentous phage, and the detecting principle of ME biosensor.

Chapter 4 shows the concept and fabrication of the 3D filter 1.0. The capturing performance of the 3D filter 1.0 is explored.

Chapter 5 demonstrates the capturing and filtering capability of *Salmonella typhimurium* by E2 phage-immobilized ME filter elements in the 2D filter before the development of the 3D filter 2.0.

Chapter 6 introduces the theory and system of the 3D filter 2.0, including the initial 3D filter, the large-scale 3D filter, and the multipipe-3D filter. The experiments and simulations about the capture and filtration of *Salmonella typhimurium* from large volumes of liquids with high throughput are conducted by the 3D filter 2.0 system with E2 phage-immobilized ME filter elements.

Chapter 7 presents an overall summary, conclusions, and future work of this research.

Chapter 2

## 2. Reviews of pathogen detection methods

Pathogen detection is momentous for food safety. Pathogen detection methods are used to detect whether the fresh food is contaminated by foodborne pathogens and distinguish categories of foodborne pathogens. Pathogen detection methods are divided into traditional detection methods and biosensing technologies. For both kinds of detection methods, bio-receptors are the critical part to recognize foodborne pathogens with high selectivity and specificity. In this chapter, bio-receptors, traditional detection methods, and biosensing technologies are introduced.

### 2.1. Bio-receptors

Bio-receptors are molecular species that utilize a biochemical mechanism for recognition, which are responsible for capturing or binding the analyte of interest in pathogen detection (Velusamy et al. 2010). In this subchapter, four major categories of bio-receptors are introduced, including antibody/antigen, nucleic acids/DNA, cellular structures/cells, and bacteriophage (phage).

#### 2.1.1. Antibody/antigen

Antibodies are commonly bio-receptors used for traditional detection methods and biosensing technologies in laboratories and commercial markets. Antibodies are Y-shaped proteins for neutralizing pathogens, such as bacteria and viruses, as shown in Figure 2.1 (Wikipedia 2020a). Antibodies may be polyclonal, monoclonal, or recombinant, depending on their selective properties and the way they are synthesized. In general, antibodies are typically formed by two large, heavy chains and two small, light chains. Different types of heavy chains define five different types of immune globulin, including IgA, IgD, IgE, IgG,

and IgM. In contrast, antigens are unique molecules of analytes of interests, which are recognized by antibodies.

The way in which an antigen-specific antibody interact is similar to a lock and key fit (Velusamy et al. 2010). A specific antibody fits its unique antigen in a highly specific manner, resulting in the match of the three-dimensional structures between antigen and antibody molecules. The paratope on each tip of the antibody is analogous to a lock. The epitope on antigen is the key, which is specific for the lock of paratope. The structure of an antigen-antibody lock and kit fit is illustrated in Figure 2.2.

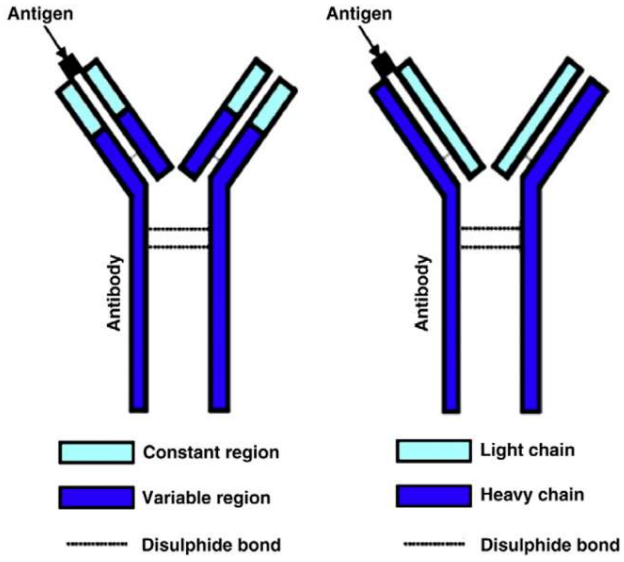


Figure 2. 1 Antibody basic structure.

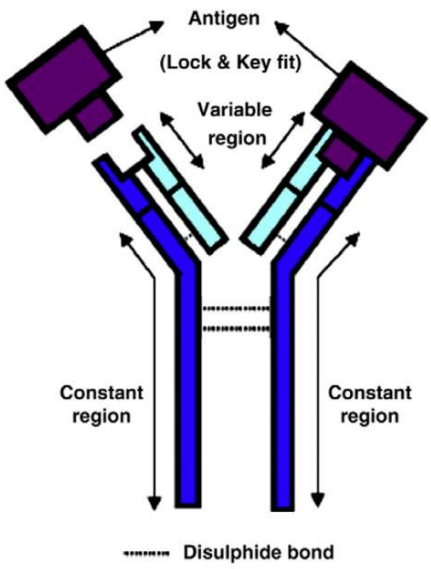


Figure 2. 2 Antigen-Antibody key and lock fit.

In general, antibodies are covalently modified with labels to suit the purpose of a particular assay. Enzymes, biotin, and fluorophores are used as labels to provide detection signals in immunological methods. Covalently attaching such a label combines the specificity of the antibody in a sensitive assay for detection, thus creating an ideal probe molecule.

### 2.1.2. Nucleic acids/DNA

For nucleic acid bio-receptors in pathogen detection, the identification of a target analyte's nucleic acid is achieved by matching the complementary base pairs that are the genetic components of an organism (Velusamy et al. 2010). Since each organism has unique DNA sequences, any microorganism can be easily identified by nucleic acids. Due to the simple and inexpensive characteristics, nucleic acids-based biosensors have been applied in multiple areas, including physical, chemical, and biological activities, and focused on foodborne pathogen detections, such as *E. coli* O157: H7 (S. H. Chen et al. 2008) and *Salmonella spp* (Lermo et al. 2007).

However, DNA damage is an essential factor to be considered when nucleic acid bio-receptors are used. Chemical detection may cause irreversible damage for base sequence and structure of DNA, and in turn, disturb the DNA replication.

In recent research, peptide nucleic acid (PNA) has been developed as another kind of bio-receptor. PNA is a synthesized DNA in which the sugar-phosphate backbone is replaced by a pseudopeptide (Velusamy et al. 2010). For PNA, the chemical and enzymatic stability and the affinity of target sequences are improved compared with nucleic acids. Also, the rapid, stable, and reliable analytical processes are established because of the different molecular structures of PNA, which enable new modes of label-free detection (Velusamy et al. 2010). However, the high cost of synthesis is the main drawback of PNA. Furthermore, long PNA oligomers, depending on their sequence, are prone to aggregation, leading to more challenges to be purified and characterized. In addition, aggregate tendency and poor solubility in water media are revealed by purine-rich PNA oligomers (Alexander A. Gall, Igor V. Kutyavin, Nicolaas M. J. Vermeulen 2003).

### 2.1.3. Cellular/Cells

Cellular bio-receptors are based on whole cells or specific cell components to bind target species. In cellular systems, the recognition and response are realized by the biochemical stimuli from detecting targets to cells. For cell-based detection methods, detected analyte is converted into a cellular response because of biochemical stimuli, resulting in an electronic signal on a transducer. As one of the bio-receptors, living cells are well-suited for recognition. Cells can provide sensitivity to a wide range of biochemical stimuli and a functional assay for biochemical agents. In addition, a low detection limit is provided to a wide range of biochemical stimuli due to signal amplification (Velusamy et

al. 2010). Although the cellular system is popular to identify and quantify the pathogenicity of foodborne pathogens by many researchers, drawbacks are still displayed. A specific environment must be satisfied to function normally for the cells. Moreover, the self-life of cells is very short, and preservation is complicated. In addition, the type of pathogens or toxins is challenging to be identified by the cellular response according to the biochemical stimuli, since multiple biochemical pathways can lead to the same cellular response (Velusamy et al. 2010).

Mammalian cells-based detection methods to detect foodborne pathogens were developed because a manner responded can offer insight into the physiological effect of an analyte. This type of cell-based detection method can distinguish viable and nonviable pathogen cells uniquely, which is a critical determination for the food industry due to no potential threats from nonviable pathogens. The first research of the collagen-encapsulated mammalian cell-based detecting system was accomplished by Banerjee for the rapid detection of *Bacillus cereus* strains and *Listeria monocytogenes* strains (Banerjee et al. 2008). The rapid detection of viable cells of foodborne pathogens, including *Listeria*, the toxin listeriolysin O, and the *enterotoxin* from *Bacillus* species, was demonstrated by multi-well plate-based biosensor containing B-cell hybridoma, Ped-2E9, encapsulated in type I collagen matrix.

Besides the mammalian cell, the application of chromatophore cell-based sensing systems for the detection of foodborne pathogens was demonstrated by Carlyle (Carlyle CA, Svejcar M, et 2002; Velusamy et al. 2010). The chromatophores are pigmented cells extracted from betta splendens that undergo a color response, due to aggregation under the exposure of specific biologically active agents. Chromatophore cells were exposed to

purified pathogen toxins and live toxin-producing pathogen strains to test the effect of pathogen toxins. The pigmented organelles in the chromatophore cells were aggregated under the exposure of toxin-producing strains of *E. coli*, *Salmonella*, *Shigella*, *Vibrio*, *B. cereus*, and *Clostridium*. The aggregation of the pigmented organelles was not observed in the structure of chromatophore cells under the non-toxin producing strains of *E. coli*, *Bacillus subilis,* and *Lactococcus lactis*. This phenomenon indicates that the aggregation of the pigmented organelles in chromatophore cells was toxin dependent, and it is nonreversible.

Moreover, an artificial cell-based sensing system coupled with a liposome-doped silica nanocomposite was developed by Zhao to detect Listeriolysin O, a pore-forming hemolysin secreted by the foodborne pathogen *L. monocytogenes* (Zhao et al. 2006). The liposomes, containing fluorescent dyes, are cellular compartments. The fluorescent dyes are released due to the pore formation by Listeriolysin O, illustrating the presence of the toxin. This synthetic cell-based sensing system has a long self- life, and the preservation is more accessible because of non-living system in it, compared with an authentic cell-based biosensing system.

### 2.1.4. Bacteriophage

Bacteriophage is a new biorecognition element for the identification of pathogens. The size of bacteriophage is about 20-200nm, which is much smaller compared with pathogens (Velusamy et al. 2010). Based on the specific tail spike proteins on pathogens, the identification and detection of species of pathogens can be realized by bacteriophages. Recently, the application of bacteriophages for foodborne pathogen detection has been developed. Various pathogens, such as *E. coli* (Singh et al. 2009), *B. anthracis* spores

(Huang et al. 2008), and *Salmonella*, were detected by bacteriophages with different detection methods. Therefore, a new path for the development of specific pathogen detection technologies is opened.

## 2.2. Traditional detection methods

Culture and colony counting methods, immunology-based methods, and polymerase chain reaction (PCR) are the most common traditional methods to detect pathogens. Even though complicated operations and a long operating time are required, these traditional detection methods are still regarded as the gold standard for pathogen detection. Furthermore, these detection methods are also combined with biosensors to obtain more convincing results.

### 2.2.1. Culture and colony counting methods

The culture and colony counting methods are the oldest pathogen detection methods, which provides accurate results because of its high sensitivity and selectivity. The schematic diagram of dilution and spread plate methods is displayed in Figure 2.3. It is an essential subset of cytometry for research applications. To achieve high sensitivity and selectivity, different culture media are selected to detect specific pathogens. Specific pathogens are identified according to the growing condition on different culture media. Furthermore, inhibitors are employed in culture media to stop the growth of non-target pathogens. By other methods, particular colors on the growth of target pathogens were introduced, such as rainbow agar for *Salmonella* pathogens detection. The results can be detected by optical methods, mainly by ocular inspection.

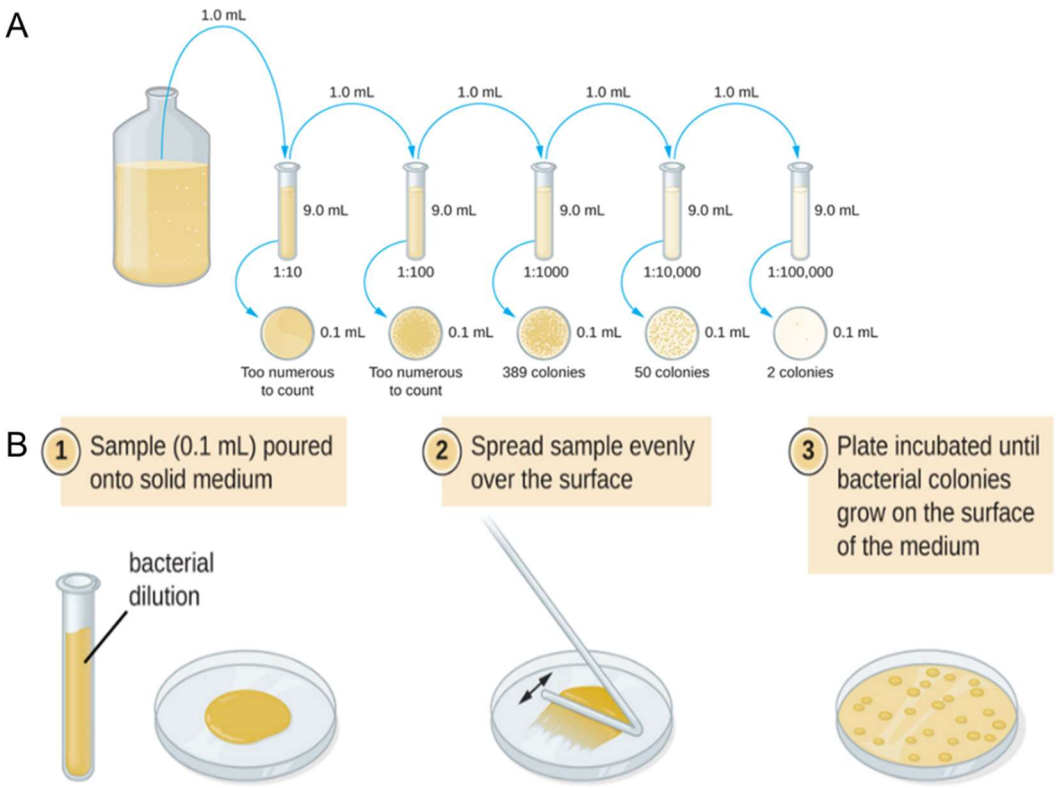


Figure 2. 3 Schematic diagrams of (A) dilution method and (B) spread plate method.

However, the major disadvantages of the culture and colony counting method are labor-intensiveness and time-consuming, since it takes 2-3 days for initial results and up to 7-10 days for confirmation. Despite the drawbacks, the culture and colony counting methods are often combined with other pathogen detection methods to verify results.

### 2.2.2. Immunology-based methods

Immunological detection methods based on antigen-antibody bindings are widely used for foodborne pathogens determination. According to the detection theory, immunology-based methods include the enzyme immunoassay (EIA), enzyme-linked fluorescent assay (ELFA), enzyme-linked immunosorbent assay (ELISA), flow injection immunoassay, and other immunological methods (Alahi and Mukhopadhyay 2017).

In these methods, ELISA test is the most established technique nowadays. The specificity of antibody and the sensitivity of enzyme are used to detect the presence of antigen. For the sandwich ELISA showed in Figure 2.4, target antigens are bound by capturing antibodies immobilized on an ELISA plate, followed by enzyme-conjugated detection antibodies. Because of enzymes, an added chemical is converted into a color or fluorescent or electrochemical signal. The absorbance or fluorescence or electrochemical signal of the pate wells is measured to determine the presence and quantity of antigen.

Compared with culture and colony counting methods, less preparing time is required. However, real-time pathogen detection is not satisfied with immunology-based methods (Alahi and Mukhopadhyay 2017; Meng and Doyle 2002).

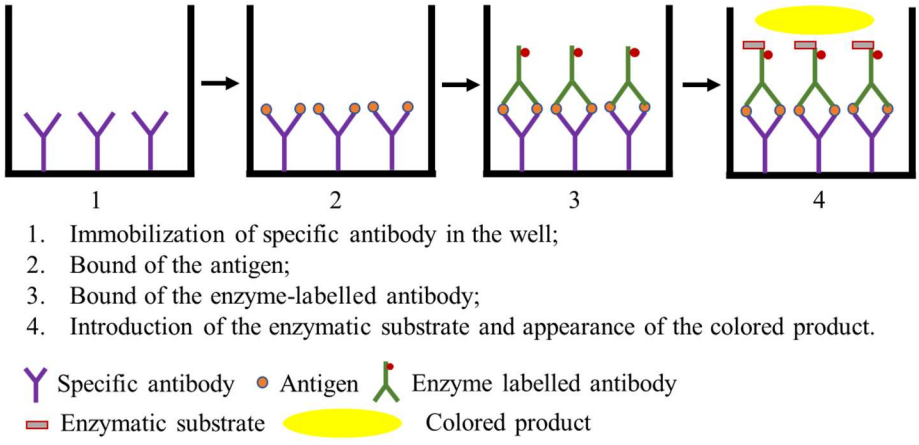


Figure 2. 4 Schematic diagram of sandwich ELISA.

### 2.2.3. Polymerase chain reaction (PCR)

PCR is a nucleic acid amplification technology consisting of isolation, amplification, and quantification of a short DNA sequence from DNA sequences of a target analyte (Lazcka, Campo, and Muñoz, 2007). This method can detect a single copy of a target DNA sequence. It is less prone to producing false-positives since pathogens are detected by amplifying target DNA sequences rather than signals. The general PCR operation is

displayed in Figure 2.5, including cycles of denaturation by heating, purified and extracted DNA, and recognition of DNA strands by primers (Lazcka, Campo, and Muñoz 2007). Then each new double-stranded DNA is used for further cycles of denaturation and amplification. After the enrichment, the amplified DNA sequences are finally detected by gel electrophoresis.

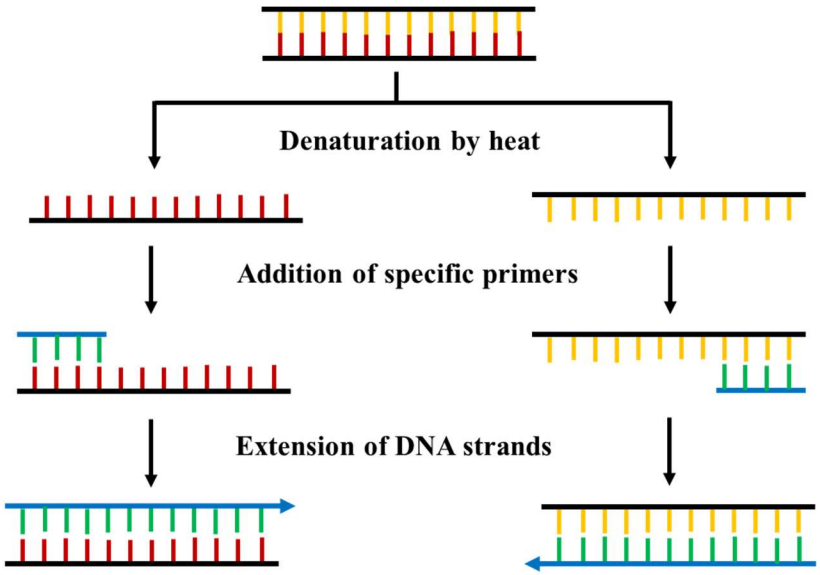


Figure 2. 5 Schematic diagram of one PCR cycle in thermal cycler.

In decade years, multiple PCR techniques have been developed, including real-time PCR, multiplex PCR, and reverse transcriptase (RT) PCR. Real-time PCR realizes much quicker results without too many manipulations. A specific dye is used to emit fluorescence from the targeted amplicon. The intensity of fluorescence is proportional to the amount of amplified product (Cady et al. 2005). For multiplex PCR, simultaneous detection of several pathogens is allowed by introducing different primers to amplify the DNA regions coding for specific genes of each pathogen strain targeted. Since viable and non-viable cells cannot be distinguished by the PCR techniques mentioned above, RT-PCR was developed to

overcome this limitation. Yaron and Matthews developed an RT-PCR to detect only viable cells of *E.coli* O157:H7 (Yaron and Matthews 2002).

### 2.3. Biosensor detection technologies

Because of time-consuming and complicated procedures of the traditional techniques for pathogen detection, rapid and easy-to-use biosensing technologies were developed. Biosensing technologies have been developed in the past decades. A biosensor is an analytical device to detect a chemical substance or microorganism by a combination of a biological component and a physicochemical detector. A biosensor consists of a bio-receptor and a transducer. A bio-receptor recognizes the target analyte, and the transducer plays an essential role in the detection process to convert the recognition event into a measurable electrical signal. The transduction can be optical, electrochemical, magnetic, and micromechanical or combinations. According to the conversion methods, the popular and common biosensors are optical, electrochemical, and mass-based biosensors, as shown in Figure 2.6.

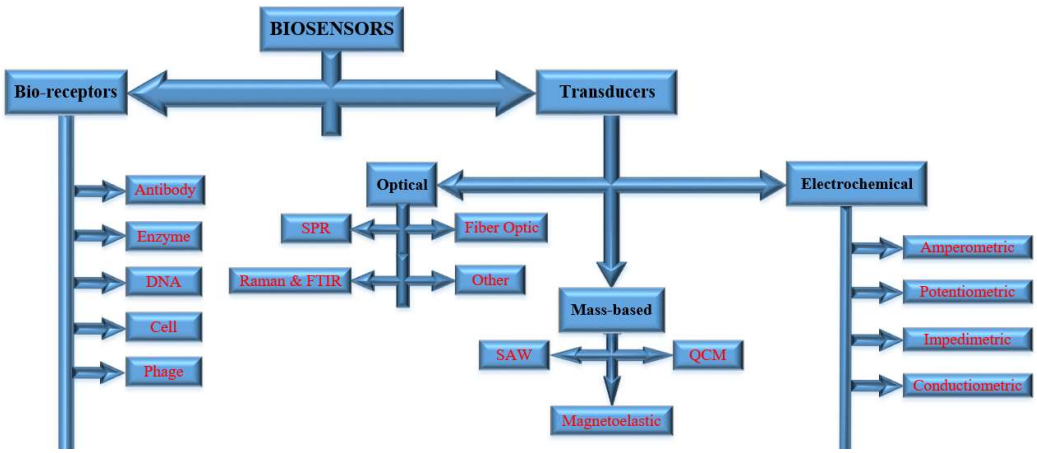


Figure 2. 6 Classification of biosensors for different transducers.

#### 2.3.1. Optical biosensors

Researchers have paid attention to optical biosensors due to their sensitivity and selectivity. Mechanisms of optical biosensors are based on absorption, refraction, reflection, dispersion, infrared, Raman, and fluorescence. For optical biosensors, a suitable spectrometer is pre-requisite to record the spectrochemical properties of analyte. The most commonly employed techniques used for optical detection are Raman and Fourier transform infrared (FTIR) spectroscopy, surface plasmon resonance (SPR), and fluorescence.

Raman spectroscopy, as fingerprinting technology, is used to detect pathogens rapidly based on light scattering. A dispersive system spectrophotometer with a 785nm diode laser is applied to detect Gram-positive and Gram-negative pathogens (Schmilovitch et al. 2005). Another detection method that uses surface-enhanced Raman scattering (SERS) microscopy for label-free transduction was developed (Grow et al. 2003). The results showed that *Listeria*, *Bacillus* spores, and *Cryptosporidium oocysts* were identified at the strain level on the basis of SERS fingerprints collected from single organisms. In addition, the pathogen detection using Raman spectroscopy without drying the microorganisms was demonstrated by Goeller and Riley (Goeller and Riley 2007).

Fourier transform infrared (FTIR) spectroscopy is a non-destructive analytical method for pathogen detection. Yu developed the FTIR spectrometry-based approach for microbial differentiation and quantification of eight different microorganisms (Yu et al. 2006). Furthermore, the differentiation of *E. coli* O157: H7 from other pathogens inoculated into apple juice was demonstrated by the use of FTIR spectrometry technique (Al-Holy et al. 2006).

Surface plasmon resonance (SPR) is another pathogen detection technique in optical biosensors. Pathogen detections, such as *Salmonella* (Bhunia et al. 2004) and *E. coli* O157: H7 (Meeusen, Alocilja, and Osburn, 2005), have been demonstrated by the SPR technique. SPR apparatuses can be designed with different setups. A glass prism commonly couples the polarized light into the sensor coated with a thin layer of gold. A flow channel for reactant flow is integrated with the thin gold layer. Both bio-receptor immobilization and analyte binding events are occurred at the interface. The intensity of reflected light is recorded by a detector with a photodiode. The variation in the refractive index on the interface is also measured in resonance units (RU). As shown in Figure 2.7 (Brogioni and Berti 2014), the angle of reflected light is shifted from position 1 to position 2 when analytes are captured by ligands in the flow channel under a defined incidence angle. The angular variations with time are plotted by the resonance units. It indicates that the change in the composition of the medium on the thin gold layer is resulted from the reaction between analytes and bio-receptors.

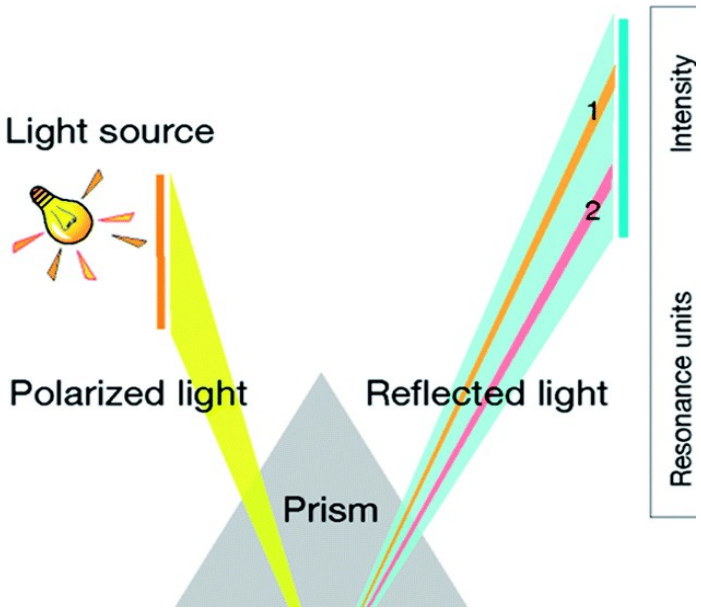


Figure 2. 7 Schematic diagram of SPR.

The use of multi-channel SPR biosensors for the simultaneous discrimination of multiple target analytes from mixtures was demonstrated by Taylor (Taylor et al. 2006). Using an eight-channel SPR biosensor based on wavelength division multiplexing, the quantitative and simultaneous detection of the four species of pathogens, including *E. coli* O157:H7, *Salmonella*, *L. monocytogenes*, and *C. jejuni*, was demonstrated. Secondary antibodies were used to amplify the result of simultaneous detection in a complex mixture of different species of pathogens, to achieve a lower detection limit. The results illustrated that specific pathogen detection in a mixture of different species of pathogens can be achieved using secondary antibody amplification.

### 2.3.2. Electrochemical biosensors

Electrochemical based detection techniques are another way of transduction to identify and quantify foodborne pathogens. Electrochemical biosensors can be divided into

amperometric, potentiometric, and impedimetric, according to the different types of observed signal responses.

Amperometric biosensors are the most common electrochemical detection methods with high sensitivity. For amperometric biosensors, the applied potential, where the analyte produces current, is the driving force for the electron transferring reaction. And then, the current is a direct parameter for the rate of transferring electron. Foodborne pathogens detection with the amperometric biosensor has been reported by many researchers, such as *E. coli* O157: H7 (Abdel-Hamid et al. 1999a; 1999b; Ruan, Wang, and Li 2002), *Salmonella* (Ruan, Wang, and Li 2002; Yang, Ruan, and Li 2001), *C. jejuni* (Chemburu, Wilkins, and Abdel-Hamid 2005), and *L. monocytogenes* (Chemburu, Wilkins, and Abdel-Hamid 2005; Crowley, O'Sullivan, and Guilbault 1999). Amperometric biosensors were also found coupled with other biosensing techniques. Pathogen detections, like *E. coli* O157: H7 (Ruan, Wang, and Li, 2002) and *Salmonella typhimurium* (Yang, Ruan, and Li, 2001), were demonstrated by bio-enzyme amperometric biosensors coupled with immunomagnetic separation techniques.

For potentiometric biosensors, the bio-recognition process between target analytes and bio-receptors is converted to a measured potential signal. A high impedance voltmeter is used to measure the electrical potential difference between two electrodes at near-zero current. Since a logarithmic concentration response is generated from potentiometric detection methods, a tiny concentration change of analytes can be detected. The detection of *E. coli* from vegetable food was demonstrated by the potentiometric alternating biosensing (PAB) system, based on a light addressable potentiometric sensor as a transducing element (LAPS) (Ercole et al. 2003). The LAPS transducer consists of a

heterostructure made of n-type silicon, silicon dioxide, and silicon nitride positioned into a measuring chamber. The insulator layer is pH sensitive due to the proton binding ability over a large pH range. Redox potential signals are measured when analytes react with the biosensor in contact with the silicon structure. Potential variations, thus, are obtained by pH variations due to $NH_3$ production by a urease-*E. coli* antibody conjugate linked with the *E. coli* cells in suspensions. The paper reported that the detection time of *E. coli* suspensions at concentrations as low as 10 cells/mL is 1.5 h for the PAB system, which was from 10 to 20 times shorter than conventional culture and colony counting methods.

Besides amperometric and potentiometric biosensors, impedance biosensors with biological recognition techniques have been developed to detect and quantify foodborne pathogens, such as electrochemical impedance spectroscopy (EIS). In the EIS system, an AC electrical stimulus between 5 mV and 10 mV is applied at a range of frequencies, resulting in a current flowing through the biosensor, depending on different processes. Compared to amperometric and potentiometric biosensors, the EIS measurements can be employed to investigate 'label-free' detection of analytes by impedimetric transduction. However, the detection limit is inferior compared with the traditional methods.

Interdigitated microelectrode-based impedimetric biosensors for rapid detection of viable *Salmonella* pathogens were reported by Yang (Yang et al. 2004). From the article, the impedance growth curves with *Salmonella* pathogen growth time were recorded at four frequencies (10 Hz, 100 Hz, 1 kHz, and 10kHz). The impedance did not change before the concentration from $10^5$-$10^6$ cfu/mL. The maximal change of impedance was detected at 10 Hz. The detection times for $4.8\times10^5$ cfu/mL and $5.4\times10^5$ cfu/mL were 9.3 hrs and 2.2 hrs, respectively.

### 2.3.3. Mass-sensitive biosensors

Mass-sensitive biosensors are based on the small change in mass, resulting in a very sensitive detection. The principle of mass-sensitive biosensing depends on the use of piezoelectric crystals. Piezoelectric crystals can vibrate at a specific frequency with an application of an electrical signal of a specific frequency. The vibrating frequency depends on the applied electrical frequency and mass loading on the crystal. Thus, the frequency of oscillation changes when the mass loading increases because of the binding of chemicals, which can be measured by an electrical device. As biosensors, the surface of mass-sensitive biosensor is functioned by bio-receptors to capture foodborne pathogens. With increasing the mass loading on the surface, the resonant frequency of mass-based biosensor is decreased, resulting in an increase of the frequency shift. Quartz is a common piezoelectric material. The mass-sensitive biosensors can be divided into two kinds, including quartz crystal microbalance (QCM) and surface acoustic wave (SAW). The QCM immunosensor with nanoparticle amplification for the rapid and real-time detection of *Salmonella typhimurium* was reported by Salam (Salam, Uludag, and Tothill 2013). The detection limit was low to 10-20 cfu/mL, and the detection time was 12 mins. Moreover, the rapid detection of *E. coli* O157:H7 by SAW biosensor was reported by Berkenpas (Berkenpas, Millard, and Pereira da Cunha 2006).

Furthermore, magnetoelastic (ME) biosensors, made of amorphous ferromagnetic material, are another type of mass-sensitive biosensors. Similar to QCM and SAW biosensors, the resonant frequency of ME biosensor is decreased due to increased mass. Since the ME biosensor is used in the research, details will be introduced in the following chapter.

### 2.3.4. Microfluidic systems

Microfluidic systems are popular and widely used as a medium to transport, mix, and separate fluids in real-time and used to control and confine fluids at the micro-scale. These are devices where patterns of microchannels are either molded or engraved. Polymers are widely used in the fabrication of microfluidic systems because of excellent biochemical performance and low cost. As a mineral organic polymer of the siloxane family, PDMS, an additive in food and lubricating oils, is one of the proper materials with advantages, including transparency, elasticity, low cost, and permeability. Besides advantages, limitation of weak chemical compatibility of PDMS decides that PDMS can be mainly used for aqueous applications.

Other materials used in the fabrication of microfluidic systems are silicon and glass. The advantages of this kind of microfluidic application lie in surface stability, solvent compatibility, and thermal conductivity. For the silicon material, the main drawback is its optical opacity in the visible electromagnetic range. The primary shortage for the glass material is high cost, compared with others.

In foodborne pathogen detections, microfluidic systems served as flow systems are coupled with other detection methods, such as PCR, magnetoresistive biosensors, and impedance-based biosensors. In Amjed's research article, multiple interdigitated electrode arrays were fabricated in microchannel and tested as impedance biosensor to effectively detect the presence of *E. coli* O157: H7 and *Salmonella typhimurium* in raw chicken products (Amjed Abdullah, Shibajyoti Ghosh Dastider, Ibrahem Jasim1, Zhenyu Shen, Nuh Yuksek, Shuping Zhang, Majed Dweik 2019). As shown in Figure 2.8, the pathogen suspensions were pumped to the focusing region for concentration, and then detected in

the detection region by impedance biosensors. The results showed that the *Salmonella* and *E. coli* O157: H7 with a low concentration of 10 cfu/mL and 13 cfu/mL could be detected in less than 1h, respectively. Dastider used the impedance-based biosensor coupled with the microfluidic system to achieve the lower detection limit of $3\times10^3$ cfu/mL in *Salmonella* detection, compared with the detection limit of $3\times10^4$ cfu/mL for the non-microfluidic biosensor (Dastider et al. 2015).

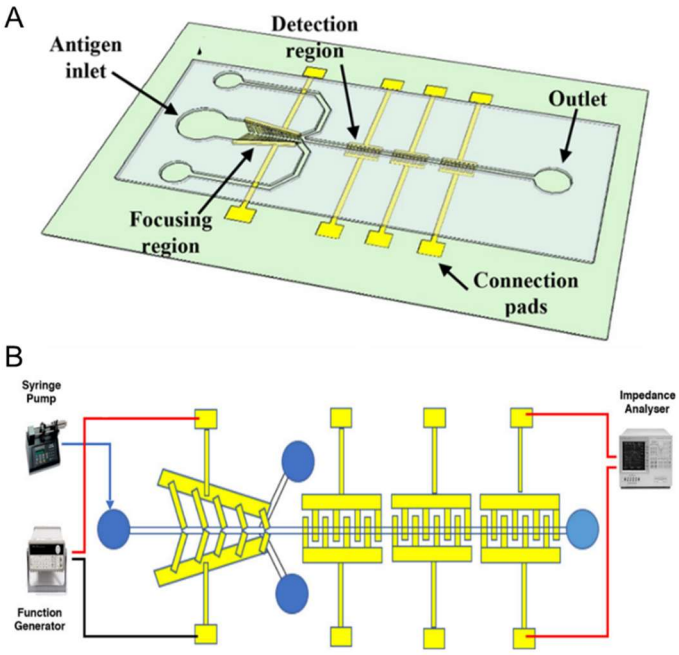


Figure 2. 8 (A) Dimensional schematic of the biosensor device; (B) Schematic of the testing setup consists of syringe pump, function generator, and impedance analyzer.

A platform of magnetoresistive based cell cytometer was explored by Fernandes (Fernandes et al. 2014). The magnetoresistive biosensor was integrated within microfluidic channels to detect magnetically labeled cells. Specific detection of *Streptococcus agalactiae* pathogens from raw milk, defatted milk, and PBS buffer was demonstrated.

### 2.3.5. Filtration methods

Besides biosensors, filtration of foodborne pathogens is another method to detect foodborne pathogens. Several filtration technologies have been developed, such as immunomagnetic beads, carbon nanotubes (CNT)-based filter, and nanofiber-based filter.

Dual-functional nisin-multi-walled carbon nanotubes (MWCNTs)-coated filter was developed to capture and inactive pathogens (Dong and Yang 2015). High permeability towards water and gases of carbon nanotubes modified filters/membranes has been reported, as well as the ability to remove pathogens from water samples, due to exceptional adsorption property of carbon nanotubes. The adsorbed nisin is a non-toxic polycyclic peptide to exhibit a broad spectrum of inhibitory activity against Gram-positive bacterial with high efficiency at nanomolar levels. The results showed that the viability of captured *B. anthracis* cells was reduced by 95.71% - 97.19%, and the metabolic activities of the captured cells were inhibited to 98.3% by the nisin deposit at the amount of 0.5 mg on the surfaces of MWCNTs. However, the testing volume was only 2 mL, and the pore size of 5 μm might result in a clogging issue, which was not suitable for large volumes of liquid streams.

Glass wool filter was also reported to concentrate viruses and pathogens, such as *Salmonella enterica* and *Cryptosporidium parvum* (Millen et al. 2012). After the initial concentration by the glass wool filter, the secondary concentration was applied for quantified recovery rate, such as real-time qPCR, immunofluorescence, and colony counting method. The glass wool filter is advantageous in that it is highly portable, available in a wide range of water matrices, inexpensive, and effective for filtering and concentrating on different types of pathogens. However, the technique is limited by defects, such as shelf-life and low filter effectiveness for high pH (>7.5) waters.

Chapter 3

# 3. Phage immobilized ME biosensor

The phage-immobilized ME biosensor consists of ME transducer and filamentous phage. The ME transducer is a platform to immobilized phage and to measure an electrical signal transferred from a resonant frequency.

## 3.1. ME transducer

The ME transducer is made of metallic glass material. The commercial product of metallic glass material (Metglas$^{TM}$ alloy 2826MB as cast) is purchased in ribbon form from Metglas. Inc. (Conway, SC, USA). This product is cast using a liquid quenching technique. To form the amorphous microstructure, the molten alloy is ejected directly on a rotating cold wheel, resulting in quick quenching freeze of the microstructure in a liquid state.

The ME transducer works under the principle of magnetostriction. The shape of ME transducer is changed with a magnetic field. This phenomenon is resulted from the rotation of magnetic domains in ferromagnetic materials along with the direction of applied magnetic field. Magnetic domains are randomly oriented in ferromagnetic materials without a magnetic field. A strain field is created because of the orientation of magnetic domains when an external magnetic field is applied, resulting in the translation from magnetic energy to elastic energy. Compared with crystalline materials, the ME material with an amorphous microstructure exhibits higher magnetic-elastic energy conversion efficiency. When an external alternating magnetic field produced by a driving coil is applied on the ME transducer, the magnetic energy is converted to mechanical oscillation with a resonant frequency, which is measured wirelessly by a pick-up coil. For a strip-shaped ME transducer with length $L$, width $w$, and thickness $t$, the ME resonator is vibrated

longitudinally with the resonant frequency. The fundamental resonant frequency ($f_0$) under longitudinal oscillation is calculated by equation 3.1 (Stoyanov and Grimes 2000).

$$f_0 = \frac{1}{2L}\sqrt{\frac{E}{\rho(1-\upsilon)}} \qquad \text{Equation 3. 1}$$

where $E$ is Yong's modulus of elasticity, $\rho$ is the density of ME resonator material, $v$ is the Poisson's ratio.

Furthermore, the ME transducer is a mass-sensitive transducer. The mass of the ME transducer increases when the target analyte is captured by a bio-receptor immobilized on the ME transducer, resulting in a decrease of the resonant frequency, as shown in Figure 3.1. The resonant frequency shift is also in proportion to the mass change of the ME biosensor. The equation of resonant frequency shift ($\Delta f$) related to the mass change of ME biosensor is shown in equation 3.2 (Grimes et al. 1999).

$$\Delta f = -\frac{f}{2}\cdot\frac{\Delta m}{M} \qquad \text{Equation 3. 2}$$

where M is the initial mass of ME biosensor, $\Delta m$ is the change in mass, and f is the initial resonant frequency.

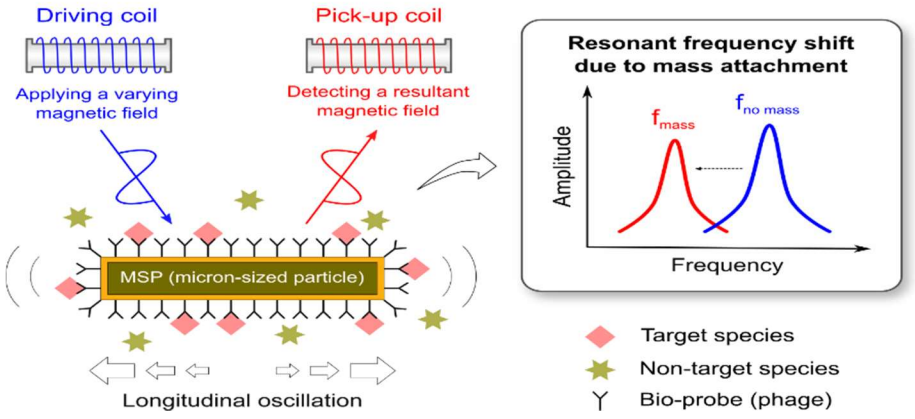


Figure 3. 1 Principle of ME transducer.

Therefore, the target analyte can be detected by measuring the resonant frequency shift of ME biosensor wirelessly.

### 3.2. Filamentous phage

The filamentous phage Ff, including fd, fi, and M13, is the main bacteriophage used in phage technology (Valery A. Petrenko 2008). It is a flexible, 800-900 nm long, thin fiber with 6.5 nm in diameter (Valery A. Petrenko 2008). The filamentous phage consists of a single-stranded DNA in the center of the body and pVIII protein coated outside of the body. Both ends of filamentous phage fd are covered with minor proteins, including pIII, pVI, pVII, and pIX (Chai 2014), as shown in Figure 3.2.

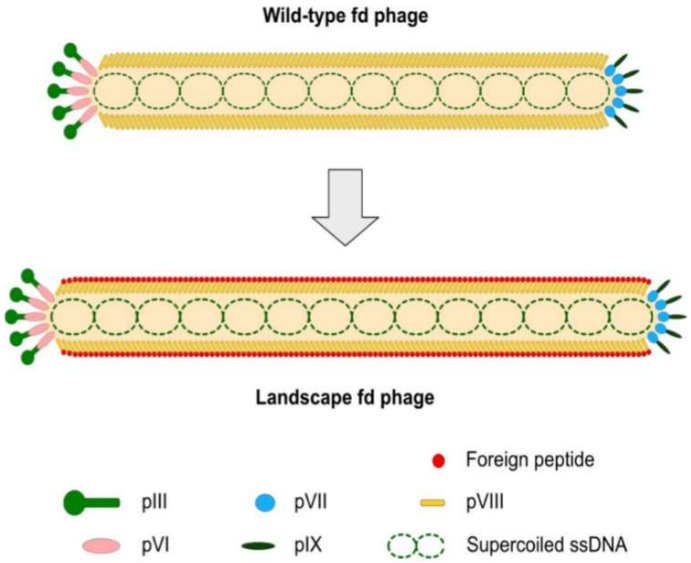


Figure 3. 2 Schematic diagram of the wild type fd phage & the landscape fd phage.

The landscape phage is recombined from the filamentous phage by adding 4000 foreign peptides on the surface (Sorokulova et al. 2005). The foreign peptides encoded by the degenerate oligonucleotides are fused to the coat protein and thereby displayed as diverse 'organic landscapes on the surface of the virions (Sorokulova et al. 2005; V. A. Petrenko et al. 2002). As the length of the virion increases in proportion when the viral

DNA is artificially lengthened by adding segments, the landscape fd phage becomes longer. Meanwhile, strong multivalent interactions with the target pathogens are achieved by the three-dimensional recognition surface with 4,000 foreign peptides binding sites.

The selected landscape phages were tested for target pathogen detection by a precipitation test, fluorescence-activated cell sorting, ELISA, fluorescent, optical, and electron microscopy (Valery A. Petrenko 2008). These tests demonstrated that the landscape phage could be used as a substitute for antibody to detect target pathogens specifically. Besides, the robustness of the landscape phage probe and antibody was compared under different temperatures, including 37 ℃, 50 ℃, 63 ℃, and 76 ℃ (Valery A. Petrenko 2008). At 37 ℃, the phage degraded slightly, but the antibody lost all of the activity in 30 weeks. At 50 ℃, both phage and antibody degraded progressively. The antibody activity was undetectable after 5 weeks, while phage still has more than 50% of activity at the same time point. At 63 ℃, the antibody was completed inactivated after 24 hrs, while the phage was stable at this temperature for 6 weeks. At 76 ℃, the binding activity of phage was still retained with a half-life of 2.4 days, even after a short incubation. These results demonstrate that the landscape phage can be functioned with highly thermostable, even exposed to high temperature in shipping, storage, and operation.

The filamentous E2 phage with highly specific and selective properties towards *Salmonella typhimurium* is engineered from a landscape f8/8 phage library (Chai 2014). The E2 phage has been shown to possess a 10-to 1,000-fold higher binding affinity for *Salmonella typhimurium* versus other pathogens. In this study, the filamentous E2 phage was used as a bio-receptor to capture *Salmonella typhimurium*.

Chapter 4

# 4. 3D phage-based biomolecular filter 1.0

## 4.1. Introduction

The first version of 3D phage-based biomolecular filter was designed to rapidly capture, concentrate, and isolate foodborne pathogens from large volume of liquid streams. The 3D filter 1.0 consisted of phage-immobilized magnetoelastic (ME) filter elements and supporting frames with solenoid coils.

The ME filter elements were served by many individual ME biosensors, which have been researched for pathogen detections about eggshell (Chai et al. 2012), tomatoes (Chai et al. 2013), chicken meat (I. H. Chen et al. 2017), spinach leaf (Park et al. 2013), water (Wan et al. 2007), fat-free milk, and apple juice (Guntupalli et al. 2007).

The solenoid coils were used to generate an electromagnetic field to align ME filter elements. The close-packed ME filter elements were aligned in openings of each supporting frame. Because of the perpendicular direction between supporting frames and electromagnetic field, ME filter elements would be aligned along with the direction of the electromagnetic field. Multiple layers of supporting frames were aligned parallelly to form multiple-layers-3D filter.

The theory of 3D filter 1.0 with the difference from the conventional bead filter is displayed in Figure 4.1. As shown in Figure 4.1, The ME filter elements are held at one end to the supporting frames by the magnetic field. The target pathogens (red dot) are captured and bound to the ME filter elements when liquids containing foodborne pathogens pass through. Meanwhile, the ME filter elements are opened like a gate to allow non-target pathogens (yellow dot) and debris (white sphere) passing through. Once the debris pass,

the ME filter elements are realigned due to the magnetic field. For the conventional magnetic bead filter, the target pathogens can be captured and filtered by the magnetic beads initially with a small volume. However, as a load of liquid stream increases, the debris in the liquid will block the pores among the beads and impede the flow in the column, resulting in an unavoidable clog issue. Therefore, the continuous flow of high throughput can be accomplished by the unique porous 3D layered structure of the anti-clogging phage-based biomolecular filter system.

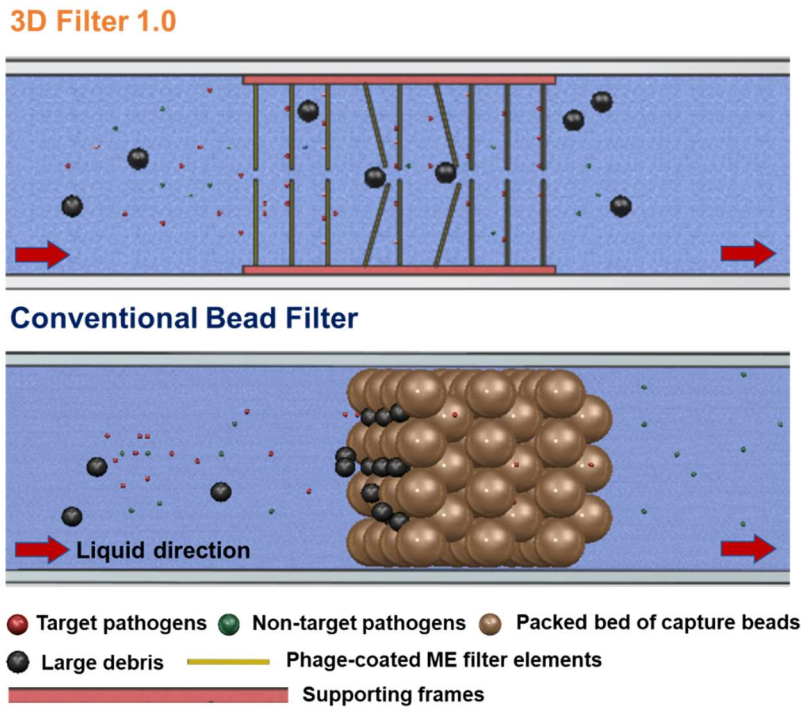


Figure 4. 1 Theory of 3D filter 1.0 with the difference from conventional bead filter.

### 4.2. Design & material selection

To align and detach ME filter elements on supporting frames, a magnetic field was used since the ME filter elements show a soft magnetic property. The supporting frames were also fabricated by a soft magnetic material with high magnetic permeability to guarantee the easy alignment and detachment of ME filter elements. The magnetic field

was realized by solenoid coils configured to the supporting frames. Figure 4.2 shows the schematic diagram of the 3D model of supporting frames with solenoid coils. The ME filter elements were magnetically coupled to the large openings of the supporting frames in a planar array to form a filter plane, as shown in Figure 4.3.

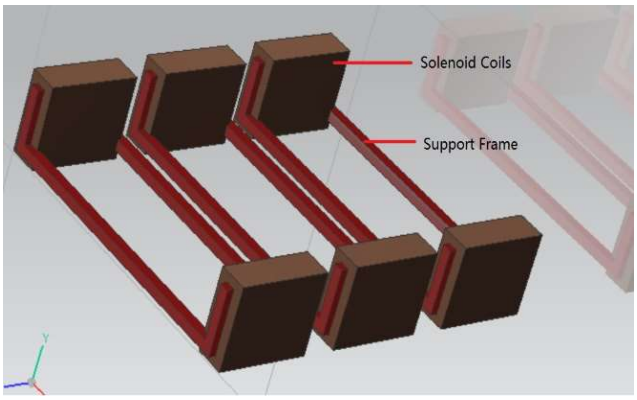


Figure 4. 2 Schematic diagram of 3D model of supporting frames with solenoid coils.

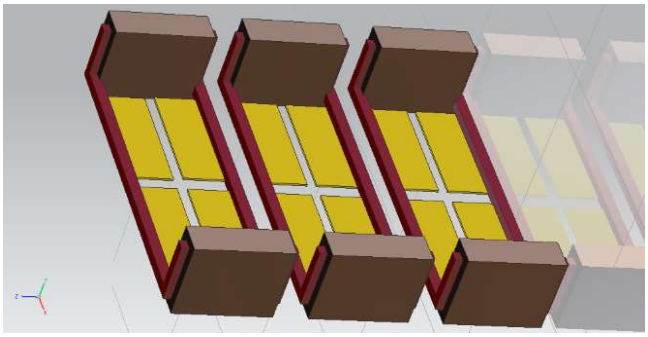

Figure 4. 3 Schematic diagram of 3D model of supporting frames with solenoid coils coupled with ME filter elements.

Soft magnetic materials are easily magnetized and demagnetized by an electric current. A magnetic hysteresis curve is a standard to verify the characteristics of magnetic materials. Soft magnetic materials are characterized by low loss and high permeability. The high permeability and low coercivity are two main parameters to select soft magnetic materials for fabrication of supporting frames. There are about seven major groups of commercially soft magnetic materials, including pure iron, iron-silicon alloys, iron-cobalt alloys, nickel-

iron alloys, and amorphous alloys, etc. From the commercial market, the soft magnetic materials with the properties of coercivity and permeability were pre-selected and listed in Table 4.1.

According to the requirement of premium soft magnetic materials, Permalloy 80 sheet with a thickness of 1mm was selected and purchased from ESPI metal Corp, Inc.

Table 4. 1 Soft magnetic materials pre-selected from the commercial market.

| Name | Coercitivity (A/cm) | 50 Hz maximal permeability for tapes of 1mm thickness |
|---|---|---|
| CRYOPERM | 0.02 | 70,000 |
| PERMENORM 5000 H2 | 0.05 | 120,000 |
| PERMENORM 5000 V5 | 0.04 | 135,000 |
| PERMENORM 3601 K5 | 0.1 | 50,000 |
| CHRONOPERM 36 | 0.05 | 50,000 |
| MEGAPERM 40L | 0.06 | 80,000 |
| MUMETALL | 0.015 | 250,000 |
| THERMOFLUX 55 | 0.4 | 50,000 |
| PERMALLOY 80 | 0.012 | 300,000 |

### 4.3. Fabrication & magnetic test

The structure and dimension of supporting frames were designed by AutoCAD software in Figure 4.4. The designed structure was fabricated from the Permalloy 80 sheet by Wire Cut Electrical Discharge Machine (WEDM) and then bent to a groove structure,

to maximize the magnetic force. After the fabrication of supporting frames, eight layers of solenoid coils with 45-50 turns were made on the supporting frames by 28 AWG copper magnet wire, as shown in Figure 4.5.

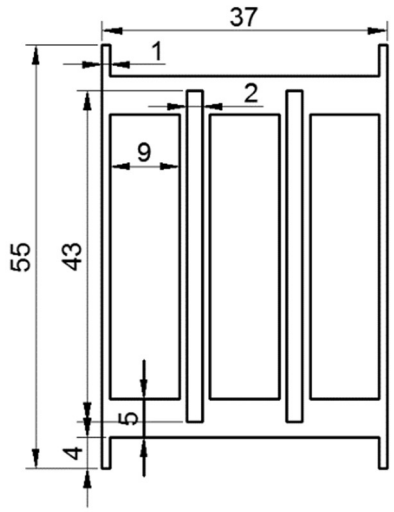


Figure 4. 4 Initial structure and dimension of supporting frames.

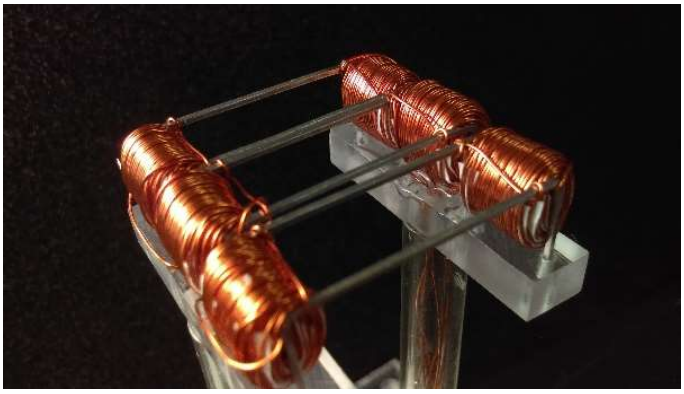

Figure 4. 5 3D filter 1.0 supporting frames with solenoid coils.

In order to achieve the magnetic field, the direct current (DC) of 1.5 A was applied on each side of solenoid coils. The magnetic force generated from solenoid coils was measured by a Gauss meter. The magnetic force of 69.72 gausses was enough to hold the ME filter elements to the supporting frames. Moreover, the magnetic field vector pattern was simulated by Ansys Maxwell. The model of the supporting frames with solenoid coils

was designed by the NX Unigraphics software. The simulating result of the magnetic field flux density vector was displayed in Figure 4.6. The magnetic flux density vector was oriented perpendicular to the vertical supporting frames so that the ME filter elements could be aligned to the supporting frames parallel with the magnetic field flux vector. The iron powder was used to double verify the simulated magnetic field flux vectors in Figure 4.7.

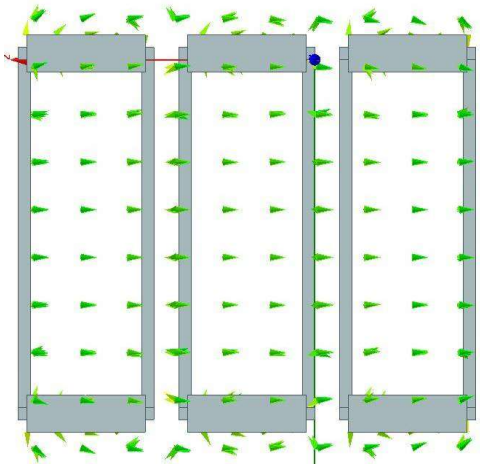

Figure 4. 6 Simulating result of magnetic field flux vector of supporting frames with solenoid coils.

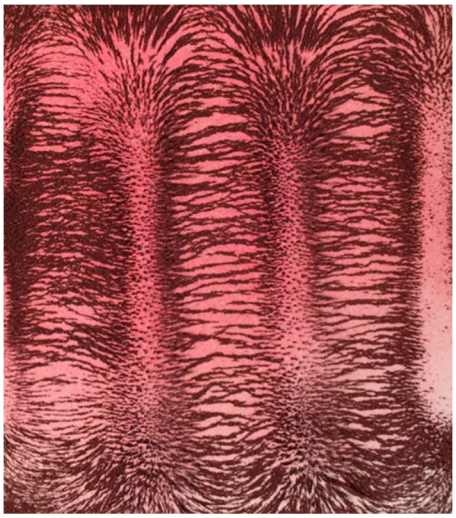

Figure 4. 7 Magnetic flux vector of supporting frames tested by iron powder.

In the 3D filter 1.0, due to the size limitation of the pipe system, the supporting frames were modified from three openings to two openings, but kept the same structure, as shown in Figure 4.8.

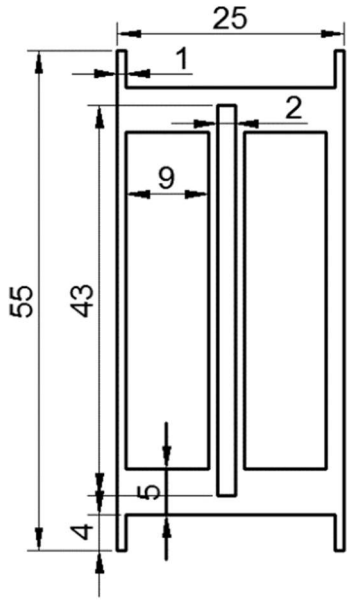


Figure 4. 8 Modified dimensions of 3D filter 1.0 supporting frames.

### 4.4. 3D phage-based biomolecular filter 1.0 system

The 3D filter 1.0 system with ME filter elements was used to explore the capture efficiency of foodborne pathogens in large volume of liquid streams, as shown in Figure 4.9. The 3D filter pipe system was constructed of a transparent food-grade plastic square pipe with an inside cross-section area of 1 inch × 1 inch, the supporting frames with solenoid coils, and a ball valve to control flow rate. The supporting frames with solenoid coils were installed into flanges to assemble and dismantle easily from the 3D filter system. The solenoid coils were set outside of the pipe to avoid the heat produced by solenoid coils. For multiple layers of the 3D filter 1.0, each layer was horizontally rotated 90-degrees

relative to the previous layer to achieve a higher contacting area between the liquid stream and ME filter elements.

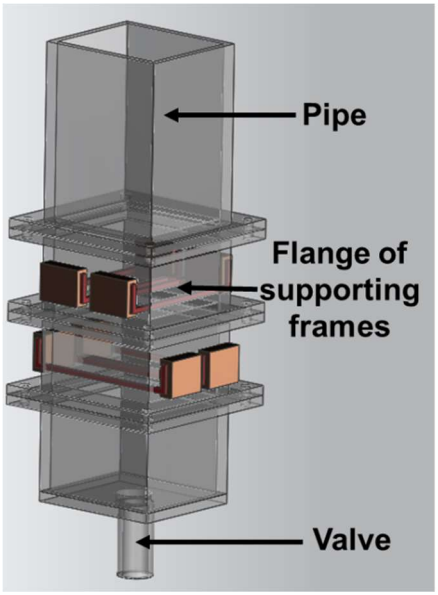


Figure 4. 9 3D phage-based biomolecular filter 1.0 system.

### 4.5. Initial test of 3D phage-based biomolecular filter 1.0

As the E2 phage and *Salmonella* pathogens might be affected by heat produced from the solenoid coils, the temperature variation of the 3D filter 1.0 system was tested, followed by the capture experiment.

#### 4.5.1. Material and methods

##### 4.5.1.1. ME filter elements

ME filter elements were fabricated from Metglas 2826MB as-cast ribbon. The raw material was diced to a rectangle-shape with a size of 10 mm×4 mm×0.03 mm. During the dicing process, an Ultraviolet (UV) sensitive film (Ultron System, Inc) was used to attach the raw material on the dicing saw (Disco 3220). After that, the diced ME filter elements were exposed under the UV light for 30 mins to release the UV sensitive film. Acetone was used to wash remnants on the ME filter elements inside an ultrasonic bath, followed

by a thorough wash in methanol. Then, the ME filter elements were vacuum annealed at 220 ℃ for 3 hrs to release residual stresses caused by the dicing process. A Chromium layer of 30 nm, followed by a Gold layer of 150 nm was sputtered to cover all the exposed surfaces of the ME filter elements. The Chromium layer was used to improve the adhesion of the Gold layer on the ME filter elements. A bioactive surface for phage immobilization and corrosion resistance was provided by the Gold layer (Park, Li, and Chin 2013).

4.5.1.2. Temperature test of 3D filter 1.0

The temperature variation of the 3D filter 1.0 system was measured, followed by the capture experiment. The temperature variation of the 3D filter system with filtered deionized (DI) water was measured by T type thermocouples in 10 mins. The T type thermocouple sensing probes were fixed at three monitoring points, including the supporting frames, above the supporting frames, and below the supporting frames. The temperature was recorded every 10 secs in the first minute and then recorded every 1 min in the next 9 mins.

4.5.1.3. E2 phage immobilization & surface blocking

The filamentous E2 phage is a genetically engineered landscape phage to capture *Salmonella typhimurium* with highly specific binding affinity and selective property (Valery A. Petrenko and Sorokulova 2004). The filamentous E2 phage with an original concentration of $1\times10^{12}$ vir/mL was prepared according to the steps presented in the previous study (Sorokulova et al. 2005). The original suspensions of E2 phage were diluted to $10^{11}$ vir/mL by Tris Buffered Saline (TBS, 1×) solution. ME filter elements were incubated with the suspensions of diluted E2 phage on a tube rotator with a speed of 8 rpm for 1 hr. After that, the phage-immobilized ME filter elements were incubated with a super

blocking buffer (1×, Thermo Fisher Scientific) for 40 mins to avoid non-specific binding on the surfaces of the ME filter elements. After surface blocking, the ME filter elements were washed once by the TBS solution and the filtered deionized (DI) water, respectively, and ready for use in the capture experiment.

4.5.1.4. 3D filter 1.0 for pathogen capture

The suspensions of *Salmonella typhimurium* with an original concentration of $5\times10^8$ cfu/mL were cultured in LB broth and prepared as described in the previous study (Sorokulova et al. 2005). The stock suspensions of *Salmonella* were further diluted to $5\times10^3$ cfu/mL. The 200 mL suspensions of *Salmonella* pathogens were prepared with filtered deionized water (DI water) and the number of *Salmonella* cells from $2.5\times10^6$ cfu to $2.5\times10^3$ cfu in it, respectively. The phage-immobilized ME filter elements were aligned on the supporting frames of the 3D filter 1.0 system. The pathogen suspensions were passed through the testing system at a flow rate of 3 mm/s once. A single layer, double layers, and triple layers were tested in this experiment. In order to determine the total number of *Salmonella* pathogens in suspensions, the plate count method was conducted on the original pathogen suspensions. After the sample loading, the ME filter elements were collected by turning off the DC power for capture rate calculation. The ME filter elements were incubated with 0.15 mL hydrochloric acid (HCl) in a 1.5 mL centrifuge tube for 10 mins to detach the *Salmonella*-phage complex from the surfaces of ME filter elements. And then, 0.05 mL Tris-HCl buffer was added and vortexed with HCl to adjust the pH of the washing solution. Since a pH indicator, Phenol Red, was used in the HCl solution, the color of the washing solution was changed from yellow to pink when the Tris-HCl buffer was mixed, and the pH value reached about 7. After that, 0.1 mL of the washing solution was spread

on culture dishes to calculate the number of capture *Salmonella* pathogens. The capture rate was calculated by the ratio of the number of captured *Salmonella* pathogens to the total number of *Salmonella* pathogens in pathogen suspensions.

### 4.5.2. Results and discussion

#### 4.5.2.1. Temperature variation of 3D filter 1.0

The temperature variations of the 3D filter system were measured in three monitoring points, including supporting frames, above the supporting frames, and below the supporting frames. The average temperatures and standard deviations of the three monitoring points were listed in Table 4.2, and the temperature variation was displayed in Figure 4.10. The temperatures of the three monitoring points increased gradually with time in Figure 4.10, respectively. But the temperature was still in the room temperature range for each monitoring point. Meanwhile, the tiny change was also verified by the standard deviation of less than 1 ℃. According to the average temperature of three monitoring points, the difference among them was less than 2 ℃. Furthermore, the flowing time of pathogen suspensions in the capture experiment was limited in 1-2 mins, which was far less than 10 mins, so that the heat effect could be neglected in the 3D filter 1.0 system. Therefore, the 3D filter 1.0 system was temperature stable for capture experiments.

Table 4. 2 Average temperature and standard deviation of temperature variation in 3D filter 1.0 system.

| | Average Temperature (℃) | Standard Deviation (℃) |
|---|---|---|
| Temp above filter | 22.31 | 0.27 |

| | | |
|---|---|---|
| (°C) | | |
| Temp of filter (°C) | 23.45 | 0.67 |
| Temp below filter (°C) | 22.53 | 0.34 |

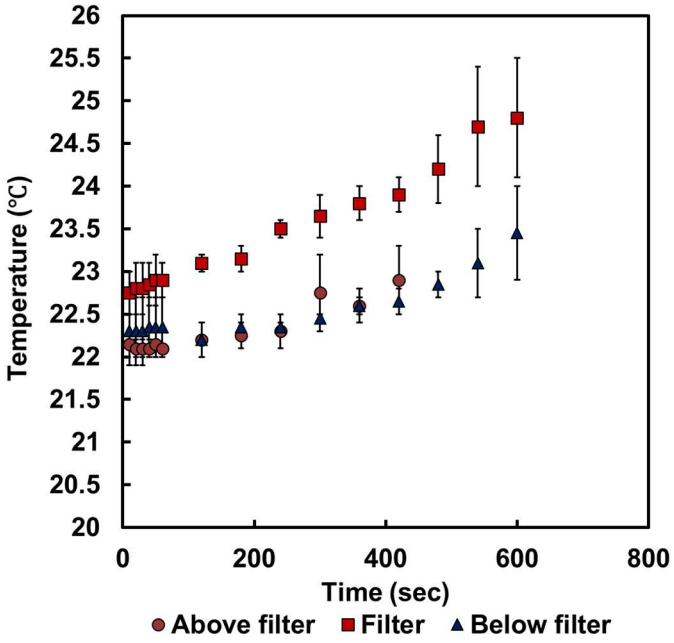


Figure 4. 10 Temperature variation of three monitoring points in the 3D filter 1.0 system.

4.5.2.2. 3D filter 1.0 capture experiment

In the initial test of 3D filter 1.0, a single layer, double layers, and triple layers of filter system were explored for the different numbers of *Salmonella* pathogens input, respectively. The capture rate results are displayed in Figure 4.11.

As shown in Figure 4.11, the tendency of capture rate can be observed obviously. The capture rate of *Salmonella* cells increased with increasing the number of filter layers for the different amounts of *Salmonella* pathogens, respectively. Due to the horizontal rotation

of 90 degrees for each layer, the coverage percentage of ME filter elements in the 3D filter system was increased, resulting in the increased capture rate. Such an increase can be attributed to the larger exposed surface area with more ME filter elements. Thus more binding sites and the higher binding possibility of *Salmonella* cells to the immobilized phage on the ME filter elements were provided. Different from other capture rates, the 0% capture rate of the single layer was displayed. The false appearance resulted from the detection limit of the plate count method and the 90% killing rate by the HCl solution, leading to no *Salmonella* cells displayed on culture dishes.

Furthermore, the increased capture rate percentage of the second and third layers based on the single layer was calculated and listed in Table 4.3, respectively. More than 100% of the increased capture rate percentage for each layer was achieved compared with the capture rate of the single layer. In addition, the growth rate also increased by increasing the number of filter layers. The increased exposed surface area of more ME filter elements and more number of filter layers is anticipated as significant factors to impact on the capture efficiency.

However, the filtration of *Salmonella* pathogens was not realized due to the low capture rate. Besides the low capture rate, the interaction between the electromagnetic field of each filter layer might affect the alignment of ME filter elements on the supporting frames if the spacing between each filter layer was too small. Based on that, the spacing between each filter layer has to be increased to minimize the effect on the alignment of ME filter elements, resulting in decreasing the density of aligned ME filter elements. In order to obtain a close-packed structure of ME filter elements, the solenoid coils were substituted by a pair of permanent magnets in the 3D filter 2.0 system.

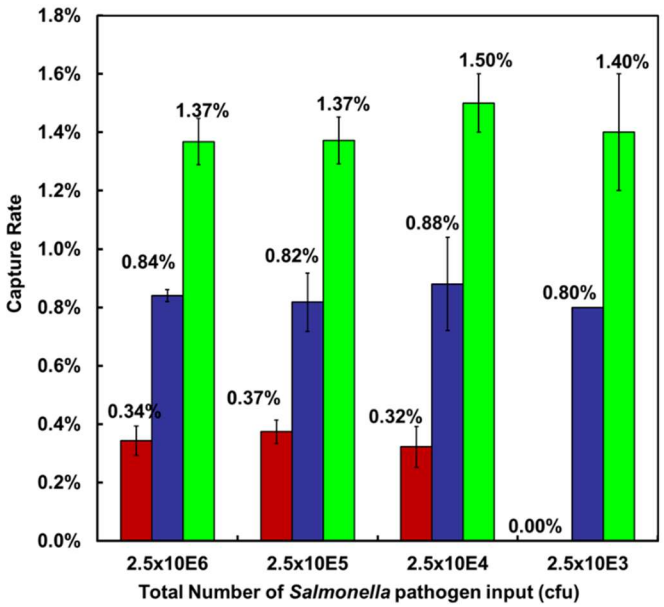


Figure 4. 11 Capture rates of S*almonella* cells with the number of 3D filter layers under different *Salmonella* cells input.

Table 4. 3 Increased capture rates percentage compared with the single layer.

| | | $2.5x10^6$ cfu | $2.5x10^5$ cfu | $2.5x10^4$ cfu |
|---|---|---|---|---|
| Increased percentage per layer | Double layers | 144.90% | 118.72% | 173.29% |
| | Triple layers | 153.94% | 148.13% | 192.55% |

### 4.6. Conclusions

In this chapter, the concept of 3D phage-based biomolecular filter 1.0 system was introduced. The structure of supporting frames with solenoid coils was confirmed, and the material of the supporting frames, Permalloy 80 alloy, was selected. The 3D filter 1.0 system with flange structures was fabricated to explore the temperature variation and then the capture experiments. The temperature variation of less than 2 ℃ demonstrated that *Salmonella* pathogens and the robustness of E2 phage were not affected by the heat produced from the solenoid coils. For the capture rate performance of the 3D filter 1.0 system, the increased capture rate was displayed with an increased number of filter layers.

Therefore, the 3D filter 1.0, coupled with ME filter elements, can be used to capture *Salmonella* pathogens in large volume of liquid streams.

However, even though the capture rate increased, the low capture rate indicated that the filtration of *Salmonella* pathogens from large volume of pathogen suspensions was not realized by the 3D phage-based biomolecular filter 1.0 system. Furthermore, the close-packed structure of aligned ME filter elements was not allowed due to the interaction between the electromagnetic field of each filter layer. Hence, a 3D filter 2.0 system was developed to explore the capability of capturing, concentrating, and isolating foodborne pathogens in large volume of liquid streams.

Chapter 5

# 5. The capability of *Salmonella Typhimurium* filtration by ME filter elements

## 5.1. Introduction

Since the experiment of pathogen filtration was never tested by phage-immobilized ME elements before, the capability of filtering *Salmonella* pathogens by ME filter elements was explored by 2D filter experiments, followed by the development of 3D filter 2.0 system. The 2D filter experiment is a popular used off-set testing method for pathogen detection in laboratories to obtain almost ideal results. In this chapter, the capability of *Salmonella typhimurium* filtration by ME filter elements is discussed.

## 5.2. Material and methods

The preparation of ME filter elements (fabrication, E2 phage immobilization, and super blocking) was described in the previous chapter, excluding the size of 1 mm×0.2 mm×0.03 mm.

The suspensions of *Salmonella typhimurium* were cultured in LB broth and prepared as described in the previous paper to the concentration of $5\times10^8$ cfu/mL (Sorokulova et al. 2005). The original suspensions of *Salmonella* pathogens were further diluted to 0.2 mL suspensions of $5\times10^3$ cfu/mL for testing.

To explore the filtering capability of ME filter elements, the 2D filter experiment was designed to incubate different amounts of ME filter elements (5, 10, 20, 50, 75, 100, 125, 150, 200, 270, 370, 500, and 800) with 0.2 mL *Salmonella* suspensions in a sterile tube for 30 mins on a platform laboratory shaker, as shown in Figure 5.1. The ME filter elements were aligned separately in the *Salmonella* suspensions by the magnetic force produced from the permanent magnet. In this way, the surfaces of ME filter elements were exposed

in *Salmonella* suspensions maximally. After that, the pathogen suspensions with unbound *Salmonella* cells were collected and transferred to another new sterile tube. Plate counts were conducted on *Salmonella* suspensions before incubation and suspensions with unbound *Salmonella* pathogens after incubation to determine the capture rates for the different number of ME filter elements.

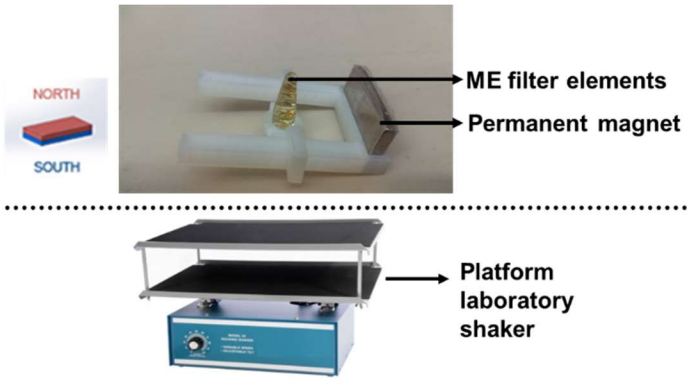


Figure 5. 1 ME filter elements were aligned separately in pathogen suspensions by permanent magnet and incubated on a platform laboratory shaker.

### 5.3. Results and discussion

The capture rate of the 2D filter experiment as a function of the number of ME filter elements is displayed in Figure 5.2. The capture rate increased with increasing the natural logarithmic value of the number of ME filter elements. The capture rate of 98% was achieved by 800 ME filter elements. The increase could be attributed to the increased surface area with more ME filter elements, thus more binding sites and the higher binding possibility of *Salmonella* cells to the immobilized E2 phage on the ME filter elements. The result demonstrated that the *Salmonella* pathogens could be captured and filtered by a certain number of E2 phage-immobilized ME filter elements in *Salmonella* suspensions.

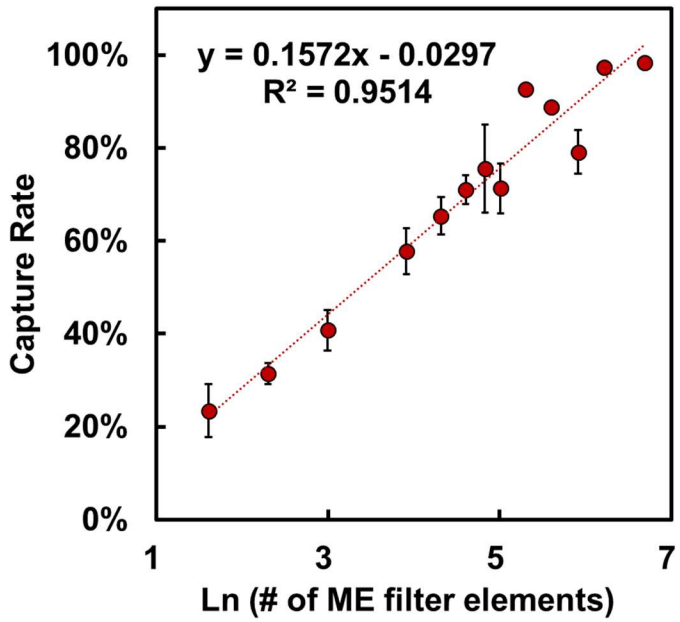


Figure 5. 2 Capture rate of the 2D filter experiment as a function of the number of ME filter elements.

### 5.4. Conclusions

In this chapter, the capability of capturing and filtering *Salmonella* pathogens was demonstrated by the 2D filter experiment. Based on the capability of filtration, the 3D phage-based biomolecular filter 2.0 system was developed and explored in the following chapter.

Chapter 6

# 6. Frameless 3D phage-based biomolecular filter 2.0

## 6.1. Introduction

The frameless 3D phage-based biomolecular filter 2.0 (3D filter 2.0) was developed to capture, concentrate, and isolate foodborne pathogens in large volume of liquid streams. The 'frameless' means that no supporting frames were used in the 3D filter 2.0 system, differing from the 3D filter 1.0 system. The 3D filter 2.0 system consisted of ME filter elements, a uniform magnetic field, and a filter pipe system.

The uniform magnetic field was produced by one pair of permanent magnetic plates to align ME filter elements in the 3D filter pipe system, instead of electromagnetic solenoid coils. Since the ME filter elements are characterized by the ferromagnetic property, the magnetic domains of ME filter elements show random directions when there is no external magnetic field. In the presence of a uniform magnetic field, the magnetic domains are all oriented with the magnetic field in one direction, resulting in an arrayed structure of ME filter elements that can be suspended and fixed in the filter pipe system. Figure 6.1 illustrates the close-packed ME filter elements in the loading pipe that exhibit unique porous 3D layered structure as compared to conventional magnetic bead filter. As shown in Figure 6.1, the gap between ME filter elements is large enough to allow debris (black sphere) and non-target pathogens (green dots) passing through, while the target pathogens (red dots) can be captured by the phage-functioned ME filter elements. For the conventional magnetic bead filter, the target pathogens can be captured and filtered by the magnetic beads initially with a small volume. However, as a load of liquid stream increases, the debris in the liquid would block the pores between the beads and occlude the flow in

the column, resulting in an unavoidable clog issue. Therefore, the continuous flow of high throughput can also be accomplished by the unique porous 3D layered structure of the anti-clogging phage-based biomolecular filter 2.0 system.

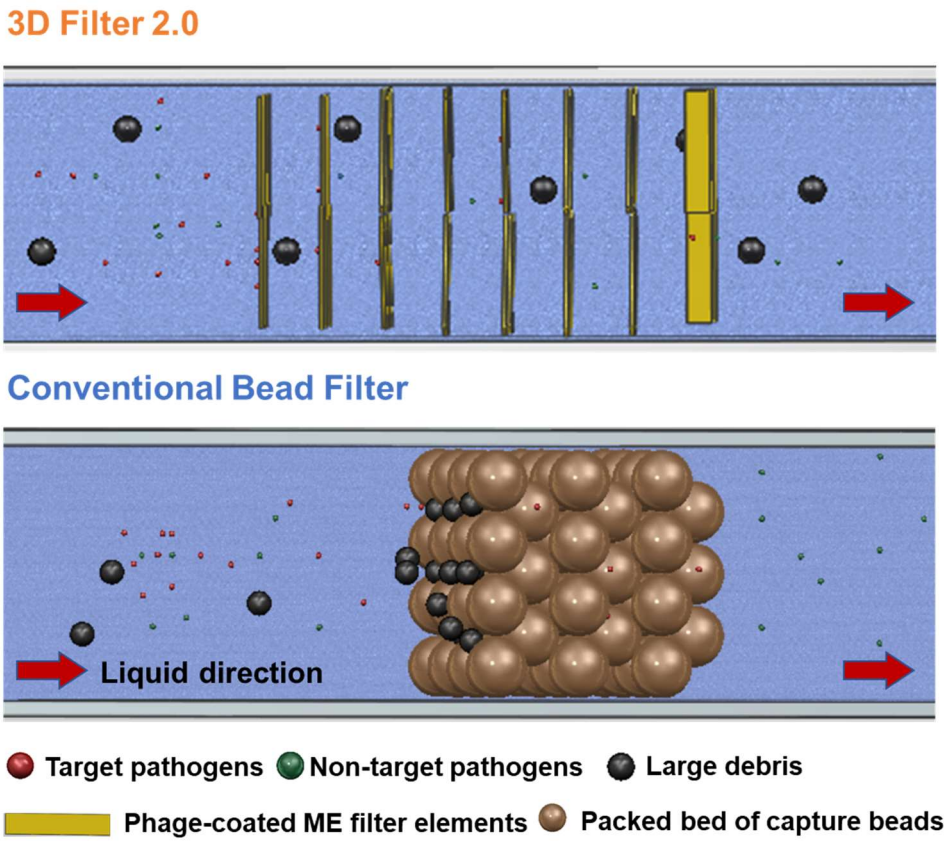


Figure 6. 1 Comparison between 3D filter 2.0 and conventional bead filter.

## 6.2. Initial test of 3D phage-based biomolecular filter 2.0

### 6.2.1. Introduction

Since the capture rate of the 3D filter 1.0 system was low for large volume of pathogen suspensions, a small volume of pathogen suspensions would be tested by the initial 3D filter 2.0 system. The pathogen suspensions of the 2D filter experiment would be tested by the 3D filter 2.0 system with the same size of ME filter elements, to compare the capture rate between the 3D filter 2.0 system and the 2D filter.

The 3D filter 2.0 consisted of ME filter elements, a uniform magnetic field, and a filter pipe system, as shown in Figure 6.2A-B. An overview of capture rates from the measurement, negative control, and blank control without ME filter elements is displayed in Figure 6.2C to indicate the high capture rate of the 3D filter 2.0 system. In this subchapter, the comparison of capture rates between the 2D filter and the 3D filter 2.0 system was discussed. The capture rates of *Salmonella typhimurium* pathogens as a function of the number of E2 phage-immobilized ME filter elements were explored by experiments and finite element analysis in the initial 3D filter 2.0 system.

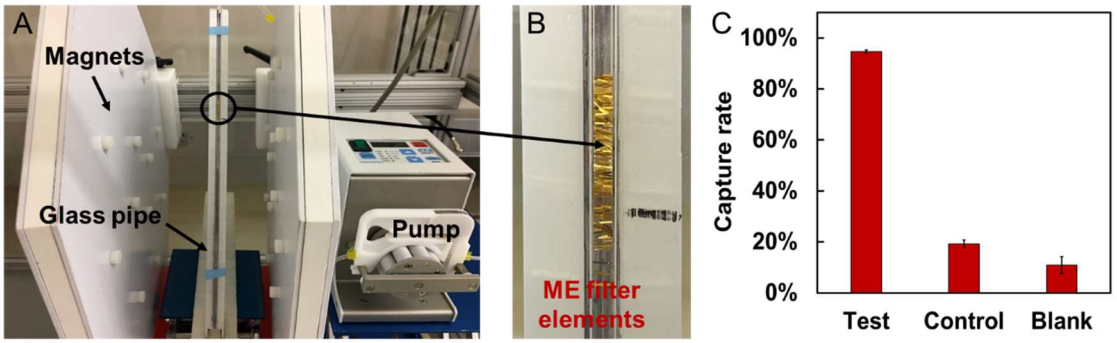


Figure 6. 2 (A) Structure of the initial 3D filter 2.0 system. (B) 3D alignment of ME filter elements coupled by magnetic field in pipe system. (C) Overview of Capture rates achieved by the phage-immobilized ME filter elements in 3D filter test, ME filter elements without phage immobilization in negative control, and blank control without ME filter elements.

### 6.2.2. Material and methods

#### 6.2.2.1. Fabrication of the initial 3D filter 2.0 pipe system

The 3D filter 2.0 system was composed of a filter pipe system with ME filter elements aligned in it by a uniform external magnetic field, as shown in Figure 6.2. The initial 3D filter 2.0 pipe system was constructed by integrating a long square glass pipe with a cross-section of 2 mm×2 mm, one pair of magnetic plates, and a flow pump. ME filter elements

with the size of 1 mm ×0.2 mm×0.03 mm were used. The ME filter elements were aligned in the square pipe by the uniform magnetic field generated by the pair of magnetic plates. The magnetic field was measured to be about 313 gausses at the center of the magnetic plates by a Gaussmeter. Because of the high surface tension of the small cross-section of the square pipe, a flow pump was used to pump the liquid samples containing *Salmonella* pathogens through the filter pipe system from the top inlet to the bottom outlet with a constant flow rate.

6.2.2.2. 3D filter 2.0 for pathogen capture and filtration

The ME filter elements' preparation is the same as the previous experiment (Fabrication, E2 phage immobilization, and super blocking), excluding the size of 1 mm×0.2 mm×0.03 mm. *Salmonella* suspensions were cultured in LB broth and prepared as described in the previous paper (Sorokulova et al., 2005) to the concentration of $5\times10^8$ cfu/mL. The stock *Salmonella* suspensions were further diluted to 0.2 mL *Salmonella* suspensions with a concentration of $5\times10^3$ cfu/mL for testing.

For the 3D phage-based biomolecular filter 2.0 system, different amount (5, 10, 20, 50, 75, 100, 125, 150, 200, 270, 370, 500, 1000, 10,000, and 20,000) of ME filter elements were arrayed into the square pipe by the uniform magnetic field, respectively. The 0.2 mL *Salmonella* suspensions were injected into the filter pipe system by the flow pump at a flow rate of 3 mm/s once. The effect of different flow rates (1 mm/s, 2 mm/s, 3 mm/s, 6 mm/s, 9 mm/s, 12 mm/s, 15 mm/s, and 18 mm/s) on capture rates was also explored by the initial 3D filter system with 100 ME filter elements. After the sample loading, plate counts were conducted on the *Salmonella* suspensions before the test and the suspensions with unbound

*Salmonella* pathogens after the test to determine capture rates for the different number of ME filter elements.

6.2.2.3.Finite element analysis

Ansys Workbench Fluent software was used to simulate the flow condition of flow domain and calculate the capture rate of the 3D filter. Turbulence and discrete particle model (DPM) were used to perform the particle tracking in liquid streams (Vahid Rastegar, Goodarz Ahmadi, S.V. Babu 2017).

The geometry of the 3D filter system, consisting of different numbers of ME filter elements and the square pipe, was designed using the Siemens Unigraphics NX software. The pipe walls were simplified to thin films with negligible thickness to predigest the numerical computation. The meshing process was conducted and plotted by Ansys Workbench Fluent software. The method of curvature function with the max face size of 0.1 mm was applied in this model. The mesh of the inlet surface was added separately to determine the number of particles in the simulation of the pathogens released from the inlet surface. In the turbulence model, the standard k-epsilon with standard wall functions was selected to analyze the flow conditions of the flow domain for general engineering calculations. The boundary conditions, including the flow velocity of 3 mm/s, the turbulent intensity of 1%, the turbulent length scale of 0.2 mm, and the DPM boundary condition type of trapping on ME filter elements' surfaces, were set and applied in the simulation.

### 6.2.3. Results and discussion

6.2.3.1. 3D filter 2.0 experiment

The capture rate of 2D filter and 3D filter 2.0 experiments with the number of ME filter elements are plotted in Figure 6.3A. As shown in Figure 6.3A, the capture rate

displays a growth with a natural logarithmic increase in the number of ME filter elements in both systems. The increase can be attributed to the larger exposed surface area with more ME filter elements, resulting in more binding sites and binding possibility on the ME filter elements. The filtering capability of the 2D filter with ME filter elements has been demonstrated in the previous chapter. For the experiment of 3D filter 2.0, the high capture rate of more than 94% was achieved. Besides, the influence of different flow rates for the capture rate is displayed in Figure 6.3B. The capture rate decreases linearly with the increased flow rate.

Interestingly, a steeper slope of the fitting function for the 2D filter system was found in Figure 6.3A, indicating the system can reach full capture capacity with a less number of ME filter elements as compared to that in the 3D filter 2.0 system. This difference could be resulting from completely different capture mechanisms in the two testing systems. As mentioned above, the 2D filter experiment on a platform laboratory shaker is a commonly used off-set testing method for pathogen detection in laboratories. Since the pathogen suspensions with the phage-immobilized ME filter elements were gently incubated and stayed almost static in the incubation process, the binding of *Salmonella* pathogens to the phage was purely based on passive diffusion. Hence, 30 mins incubation time was required for the ME filter elements to fully interact with *Salmonella* cells in the suspensions and achieve a high capture rate. It is anticipated that the required number of ME filter elements to achieve a similar capture rate of more than 90% would increase significantly under a shorter incubation time in the 2D filter system. In contrast, the liquid streams directly flowed through the 3D filter pipe system with a high flow rate using a mechanical pump in a short time. The binding events of *Salmonella* cells to the phage on the ME filter elements

can occur more frequently, but each with a much shorter interaction time as a result of the turbulent flow in the pipe. We believe that these fundamental differences between the static and dynamic interaction modes in the 2D and 3D filter systems primarily account for the distinctive fitting curves of capture rate as a function of the ME filter element number. In addition, the flow rate used in the 3D filter experiment can be another key factor that affects the capture performance of the system. As shown in figure 6.3B, even though the capture rate decreased a lot from the 1 mm/s, a higher capture rate (>45%) can be achieved at a flow rate (1-3 mm/s) with 100 ME filter elements in the 3D filter system. The capture rate decreased slightly between the flow rate of 2 & 3 mm/s. Beyond the 3 mm/s, the capture rate dropped drastically by about 5% as the flow rate increased. With increasing the flow rate in the 3D filter pipe system, the impact force produced from the high-speed liquid flow has risen. As the E2 phage was immobilized on the ME filter elements via physical adsorption, this relatively weak interaction could lead to the detach of bound *Salmonella* cells and the *Salmonella*-phage complexes from the ME filter element surfaces due to increased strong impact force. In the experiment, we used a flow speed of 3 mm/s (0.72 mL/min) as the optimal flow condition by considering both the capture rate and throughput. It is anticipated that the higher throughput can be further improved at the cost of more number of ME filter elements for the same capture rate, so that the larger number ME filter elements, which is another key factor, is anticipated to be compensated to improve the capture rate. Therefore, these results demonstrate that *Salmonella typhimurium* pathogens can be captured and filtered by the 3D phage-based biomolecular filter 2.0 system.

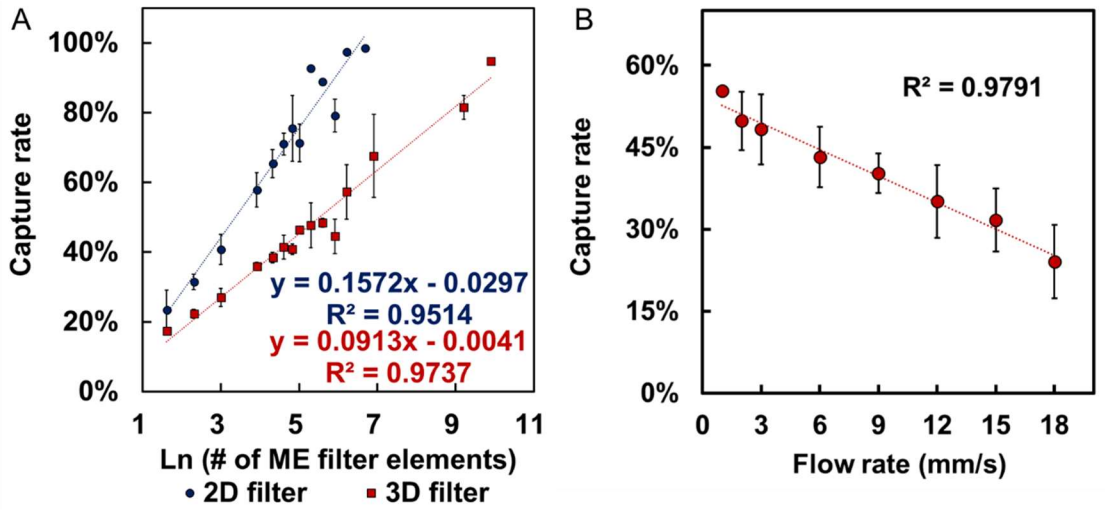


Figure 6. 3 (A) Capture rate of 2D filter and 3D filter experiments as a function of the number of ME filter elements. (B) Capture rate of 3D filter experiment with 100 ME filter elements as a function of flow rate.

6.2.3.2. Finite element analysis of flow conditions in the 3D filter system

To further understand the effect of flow condition on pathogen capture performance of the 3D filter system, we conducted a finite element analysis on turbulent kinetic energy and flow velocity generated in a simulated liquid sample loading process. In the simulation, the liquid stream was passed through the 3D structure of aligned ME filter elements in the filter pipe system. Since the ME filter elements regarded as the core component were coupled and fixed, the turbulence was produced and mixed with the liquid stream passed through the 3D filter pipe system, while the flow velocity was also changed. During the flow process, the particles similarly with the number of *Salmonella* pathogens, derived from the top inlet surface, were injected into the 3D filter pipe system, as shown in Figure 6.4A.

In the simulation results, a cross-section plane, along the sample loading direction in the square pipe, and the surfaces of ME filter elements were selected to create a contour

plot of turbulence distribution (Figure 6.4A-B), respectively. The turbulence distribution was simulated with a different number (100, 200, 370, 500, and 1,000) of ME filter elements in the 3D filter pipe system (Figure 6.4A), respectively. The contour of turbulence distribution on 200 ME filter elements' surfaces is shown in Figure 6.4B. The low turbulence distribution was displayed in the flow area without ME filter elements. While the flow area, coupled with the different number of ME filter elements, was marked by the high turbulence distribution. The turbulent intensity was also affected by the aligned structure of ME filter elements in the 3D filter pipe, which was demonstrated by the color change from green to red in the turbulence distribution of the created plane and ME filter elements' surfaces. The high possibility of pathogens hitting on surfaces of ME filter elements was provided by more contacting chance between ME filter elements and *Salmonella* pathogens in liquid stream created by the turbulence. In addition, the total turbulent kinetic energy of the created plane and the full flow domain is plotted in Figure 6.4C. The total turbulent kinetic energy increased with the increased number of ME filter elements, raising the hitting and capturing possibility for phage-immobilized ME filter elements. Meanwhile, due to the obstruction of ME filter elements in the liquid stream, flow velocity profiles of liquid stream in the 3D filter pipe system with and without ME filter elements were induced from the turbulence, as shown in Figure 6.5. The initial flow velocity was set to be 3 mm/s and remained homogenous in the 3D filter pipe system without any ME filter elements. The presence of the ME filter elements introduced strong perturbations in the liquid stream, and the flow velocity decreased drastically in the gap layer between the ME filter elements. Such the decrease of instant flow velocity induced by turbulence can also increase the capture rate according to the interaction between the

capture rate and the flow rate in Figure 6.3B. The interaction between the capture rate and flow rate has been demonstrated in Figure 6.3B that the higher capture rate was achieved by decreasing the flow rate. Therefore, the turbulence, created by ME filter elements in the pipe system, changed the flow velocity, and provided more interacting chance to increase the capturing possibility for phage immobilized on ME filter elements.

Moreover, to determine and compare the experimental and simulated capture rate of the 3D filter, the simulated capture rate by designing the different number of ME filter elements in the 3D filter pipe system was performed and calculated in Figure 6.6. Based on the boundary condition applied to ME filter elements, the released particles were randomly hit and trapped by ME filter elements' surfaces. The equivalent capture rate was calculated from the ratio of the number of trapped particles to the total number of injected particles.

In Figure 6.6, the capture rate also displays a growth with a natural logarithmic increase in the number of ME filter elements in both experiment and simulation. A higher slope of fitting function for the simulation was achieved compared with the slope of fitting function for the experiment. This difference could be expected by the different binding mechanisms between the experiment and simulation of the 3D filter. In the experiment of 3D filter system, only *Salmonella* cells captured and attached by ME filter elements were calculated. As mentioned above, due to the relatively weak interaction of physical adsorption between E2 phage and ME filter elements, the bound *Salmonella* cells and the *Salmonella*-phage complexes might be detached from the ME filter elements' surfaces by the impact force caused from the high-speed liquid flow. In the simulation of 3D filter system, the capture rate was calculated directly by the trapping boundary condition of ME

filter elements' surfaces to capture injected particles. The E2 phage was not introduced and functioned in the simulating process, so that the relatively weak interaction of physical adsorption between E2 phage and ME filter elements was not considered. The trapped particles could not be detached from the ME filter elements' surfaces by the impact force. As a result, the simulated capture rate was higher than the experimental capture rate in the 3D filter system. Hence, the increased capture rate of the 3D filter system from the experiment has been demonstrated by the simulation. And the different binding mechanisms between experiment and simulation is the key factor for the different slopes of two fitting functions.

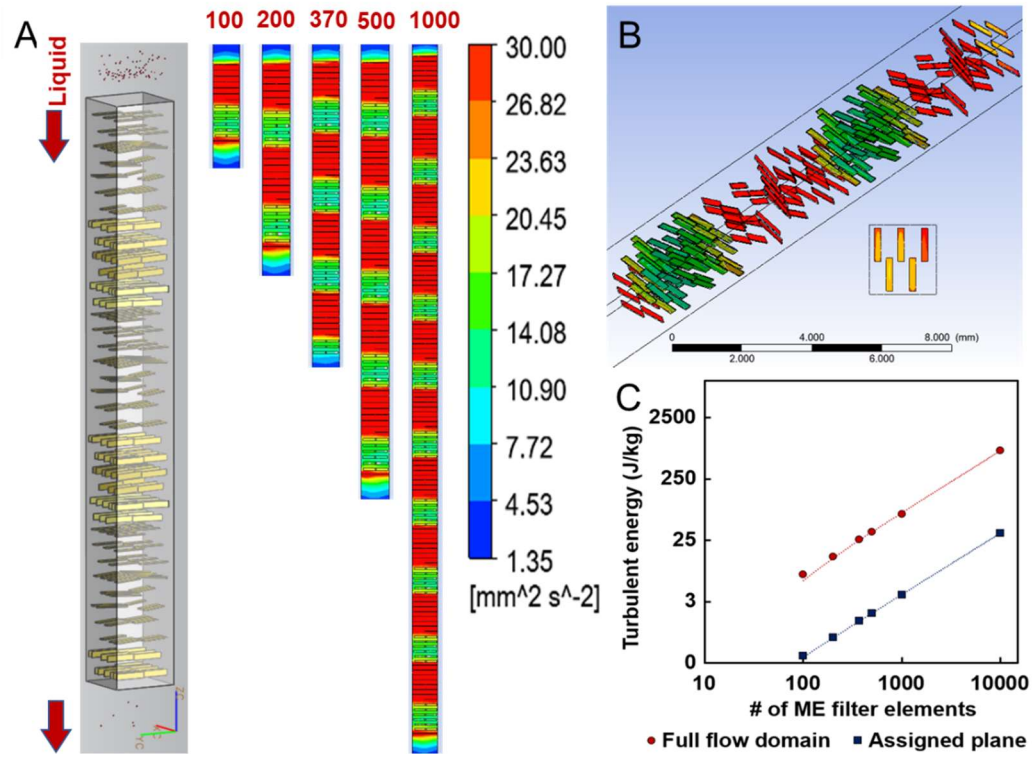


Figure 6. 4 (A) Particles as the substitute of pathogens with liquid stream were injected from the inlet of the 3D filter pipe system with aligned ME filter elements. Turbulence distribution contour on the created plan of flow liquid with the different number of ME filter elements. (B) Contour plot of the turbulence distribution on the 3D structure of 200

ME filter elements' surfaces. (C) Total turbulent kinetic energy of the created plane and full flow domain in the pipe system as a function of an increased number of ME filter elements.

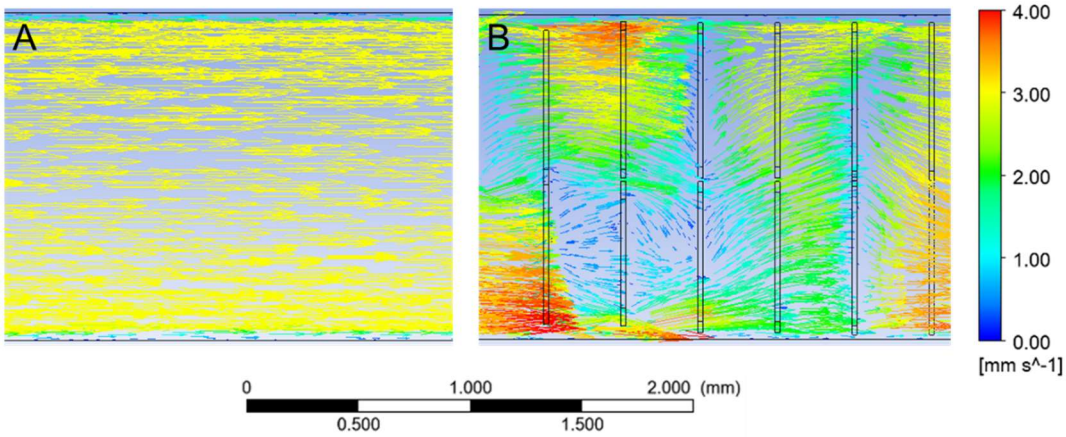


Figure 6. 5 The comparison of the varied flow velocity in the 3D filter pipe system with the ME filter elements.

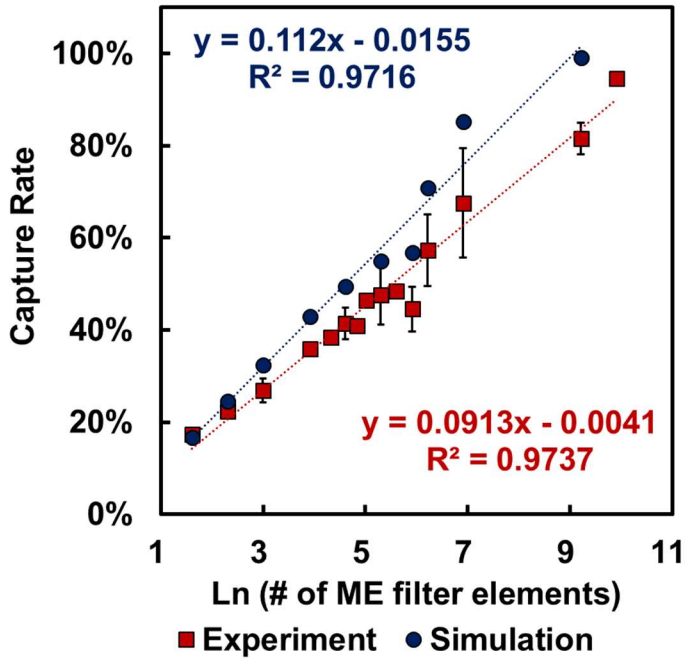


Figure 6. 6 Capture rate of the 3D filter experiments & simulations as a function of the number of ME filter elements.

### 6.3. Large-scale-3D phage-based biomolecular filter 2.0

### 6.3.1. Introduction

Since the filtration of *Salmonella* pathogens from the small volume of *Salmonella* suspensions has been demonstrated by the initial 3D filter system with 1 mm ME filter elements, the large-scale-3D phage-based biomolecular filter 2.0 system was fabricated to test large volume of pathogen suspensions in this subchapter. Different from the small cross-section of 2 mm×2 mm and making use of the flow pump in the initial 3D filter system, the large-scale-3D filter pipe system with a large cross-section area depended on gravity to pass through liquid streams. The large-scale-3D filter system was formed from the phage-immobilized ME filter elements, one pair of uniform magnetic plates, and a pipe system. The ME filter elements were still aligned and coupled in the pipe system by the uniform magnetic field. The 3D filter pipe system consisted of a square glass pipe and a ball valve to control flow rate. Large volume of pathogen suspensions were passed through the pipe system with aligned ME filter elements in it from the top inlet to the bottom outlet with a flow rate.

In this subchapter, two filter pipe systems with cross-sections of 8 mm×8 mm and 16 mm×16 mm were developed, as shown in Figure 6.7. Anti-clogging characteristic and high throughput performance were explored by the 8 mm 3D filter pipe system with 4mm ME filter elements in six testing suspensions, followed by pathogen capturing experiments as a function of the number of ME filter elements. 4 mm and 8 mm ME filter elements aligned in the 16 mm 3D filter pipe system were tested respectively to discuss the interaction between capture rate and total surface areas of ME filter elements.


Figure 6. 7 (A) 8 mm large-scale-3D filter pipe system. (B) 16 mm large-scale-3D filter pipe system.

### 6.3.2. Anti-clogging & high throughput performance

#### 6.3.2.1. Material and methods

In this experiment, the anti-clogging and high throughput performance were explored by lab water (DI water), irrigation water, thin apple juice (Kroger®, contains 25% concentrate), thin grape juice (Welch's®, contains 28% concentrate), thick apple juice (Kroger®, 100% unfiltered), and thick grape juice (Weich's®, 100% unfiltered). The DI water was from the laboratory. The irrigation water was picked from a local lake. The juices were purchased from the local supermarket. All testing suspensions were first filtered by a 125 μm filter screen to imitate the real production condition before testing.

The ME filter elements with the size of 4 mm×0.8 mm×0.03 mm were fabricated by the same method described in the previous experiment. To imitate the operation condition of pipelines in the industry, the valve-free 8 mm 3D filter pipe system was used. Figure 6.8A illustrates the 3D structure of the aligned ME filter elements in the valve-free 3D filter pipe system. To compare the flow performance of the 3D filter system, a vacuumed-

paper filter system was constructed and conducted in Figure 6.8B. The vacuumed-paper filter system consisted of a lidded conical flask, a porcelain Buchner funnel, filter papers with the function of foodborne pathogens filtration, and a vacuum system. The WHATMAN® No.5 filter paper was selected and applied in the vacuumed-paper filter system.

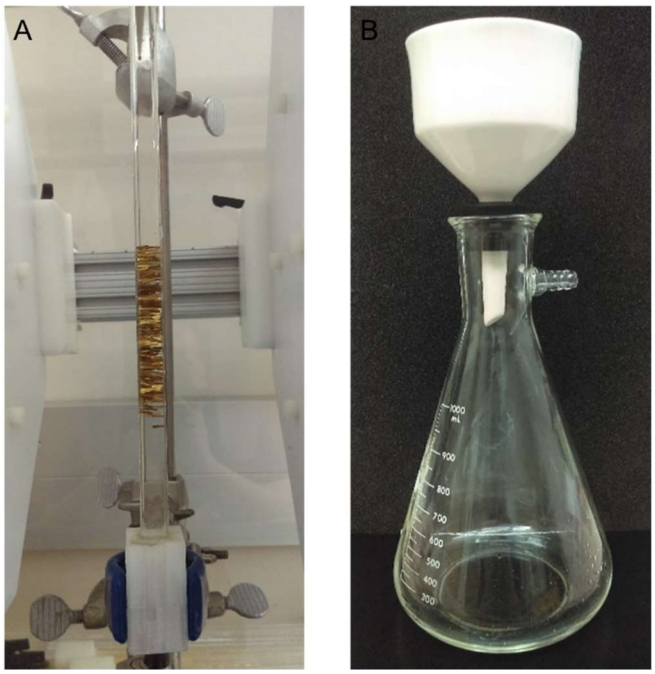


Figure 6. 8 (A) Valve-free 8 mm 3D filter pipe system with the 3D structure of aligned ME filter elements in it. (B) Vacuumed-paper filter system.

For the anti-clogging experiment, the flow time of testing suspensions was conducted as an index to explore the anti-clogging distinction between the 3D filter system and the vacuumed-paper filter system. The flow time was measured by passing through the first 100 mL from 10 L testing suspensions in the 3D filter pipe system with the different number (75, 100, 125, 150, 200, 270, 370, 500, 1,000) of ME filter elements, respectively. For the vacuumed-paper filter system, the flow time was also measured by the first 100 mL testing suspensions flowed from the funnel. To maintain constant pressure in the Buchner

funnel, the liquid level of testing suspensions in the Buchner funnel was kept at the same level.

Besides the anti-clogging experiment, the high throughput performance was also tested and compared between the 8 mm 3D filter pipe system with 5,000 of 4 mm ME filter elements and the vacuumed-paper filter system. For the 3D filter system, the flow volume of 4 L testing suspensions was recorded as a function of flow time. For the vacuumed-paper filter system, the flow time was recorded until the volume level of 4 L was reached or the continuous flow changed to the droplet flow. After that, micro-surfaces of paper filters were observed by a scanning electronic microscope (SEM, JSM-7000F, JEOL, Tokyo, Japan).

6.3.2.2. Results and discussion

The comparison of flow time between the 3D filter system and the vacuumed-paper filter system is displayed in Figure 6.9. Compared with the vacuumed-paper filter system, the flow time of 3D filter system was much lower. Focused on the 3D filter system, despite the number of ME filter elements in the 3D filter system increasing, the flow time for each of the testing suspensions displayed was similar. This result demonstrated that the flow time of the first 100 mL testing suspensions was not affected by the increased number of ME filter elements and the clog issue would not occur in the 3D filter system, compared with the vacuumed-paper filter system. The low flow time and the anti-clogging characteristic were attributed to the porous 3D structure of 3D filter system. The gap between ME filter elements is big enough to allow debris to pass through. In contrast, the filtering mechanism of the vacuumed-paper filter system is dependent on pores in filter papers, so the size of pores in filter papers for pathogen filtration is designed to micron

grade. The flow velocity of liquids is limited due to the micron scale pores in filter papers, resulting in the flow time increased. Moreover, debris and fibers blocked in filter papers may decrease the size of pores and then decrease the flow rate.

Interestingly, the flow time of the thick apple juice is not displayed in Figure 6.9 since the first 100 mL of the thick apple juice could not obtain in 20 mins and the continuous flow has been changed to the droplet flow. This result indicates that the flow time of the thick apple juice was much higher compared with other testing suspensions, resulting in the decreased flow rate and a clogging issue.

Furthermore, another phenomenon was found in the anti-clogging experiment, as shown in Figure 6.10. The flow time of the continuous 100 mL testing suspensions increased drastically, excluding the lab water and the thin apple juice. As the lab water is inclusion-free, no debris or fibers reduces the size of filter paper pores, resulting in the similar flow time of 100 mL lab water. For the thin apple juice, it is anticipated that the lowest concentrate percentage (25%) in the thin apple juice is not high enough to block the pores of filter papers in a small volume. Nevertheless, it can be expected that the flow time of 100 mL thin apple juice will be increased with more volumes.

Besides the anti-clogging experiment, the high throughput performance of the 3D filter system was also explored and compared with the vacuumed-paper filter system. The flow volume as a function of flow time for the 3D filter pipe system with 5,000 ME filter elements and the vacuumed-paper filter system is displayed in Figure 6.11. The constant flow rate of 3D filter system for each testing suspensions was demonstrated by the linear increase of the fitting functions, showing no clogging issue occurred in the 3D filter system. In contrast, the decreased slopes in the fitting functions of vacuumed-paper filter system in

Figure 6.11 illustrated that the flow rate decreased drastically with flow time, except the lab water and thin apple juice. In addition, a much more volume of testing suspensions was obtained by the 3D filter system in Figure 6.11 for the same flow time, compared with the vacuumed-paper filter system. This difference between the flow rate resulted from the clogged pores of filter papers, which were blocked by the increased quantity of debris and fibers in the continuous flowing suspensions.

The clogging issue of the vacuumed-paper filter system was also double verified by micro-surfaces of filter papers after testing suspensions passed through, as shown in Figure 6.12. The micro-surface of filter paper for lab water (B) was similar to the micro-surface of referenced filter paper (A), confirming that no debris or fibers blocked the pores of the filter paper and impeded the lab water passing through. For the thin apple juice, the increased area of white color on the micro-surface of filter paper (C) was displayed to indicate that slight debris and fibers blocked the pores of the filter paper and gradually decreased the flow rate. This result was confirmed by the decreased slope of the fitting function for the thin apple juice in Figure 6.11. In Figure 6.12, most of the micro-surfaces of filter papers (D-G) were changed into the white color, and abundant debris and fibers were observed from the micro-surfaces of filter papers, leading to an extremely severe blocking in the pores and the ultra-low flow rate.

Hence, the anti-clogging characteristic and high throughput performance of the 3D phage-based biomolecular filter 2.0 has been demonstrated, compared with the vacuumed-paper filter system.

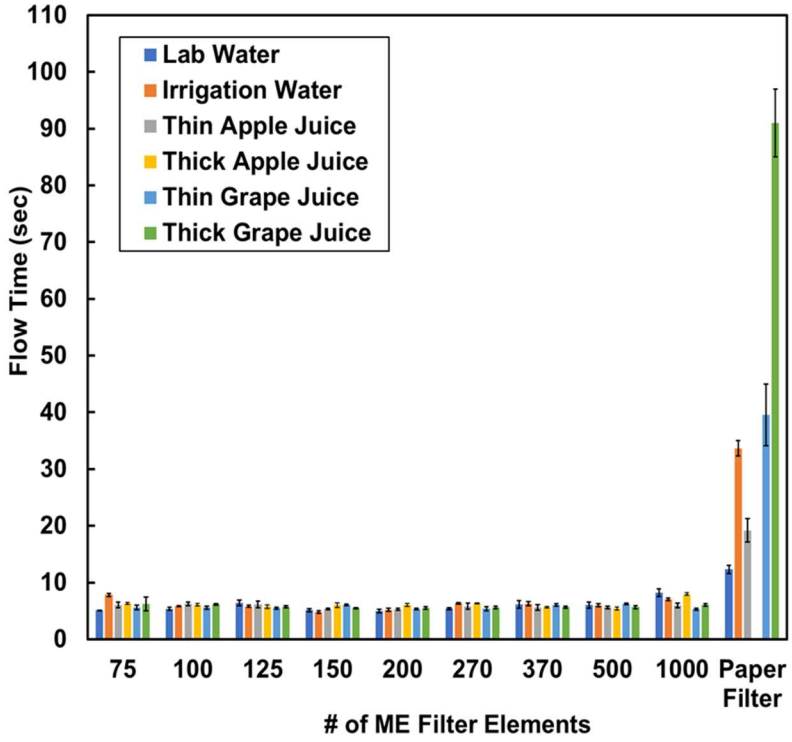


Figure 6. 9 Flow time of 3D filter pipe system with the number of ME filter elements & vacuumed-paper filter system for the six testing suspensions.

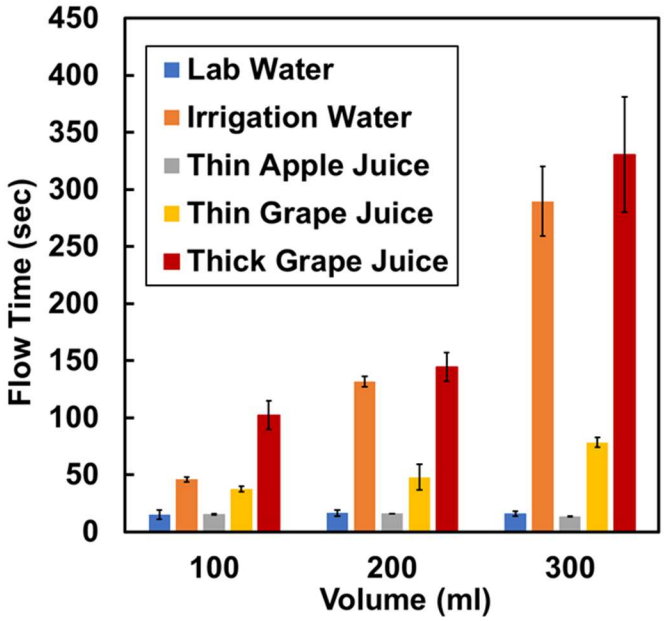


Figure 6. 10 Flow time variation of the 100 mL testing suspensions with flow volume in the vacuumed-paper filter system.

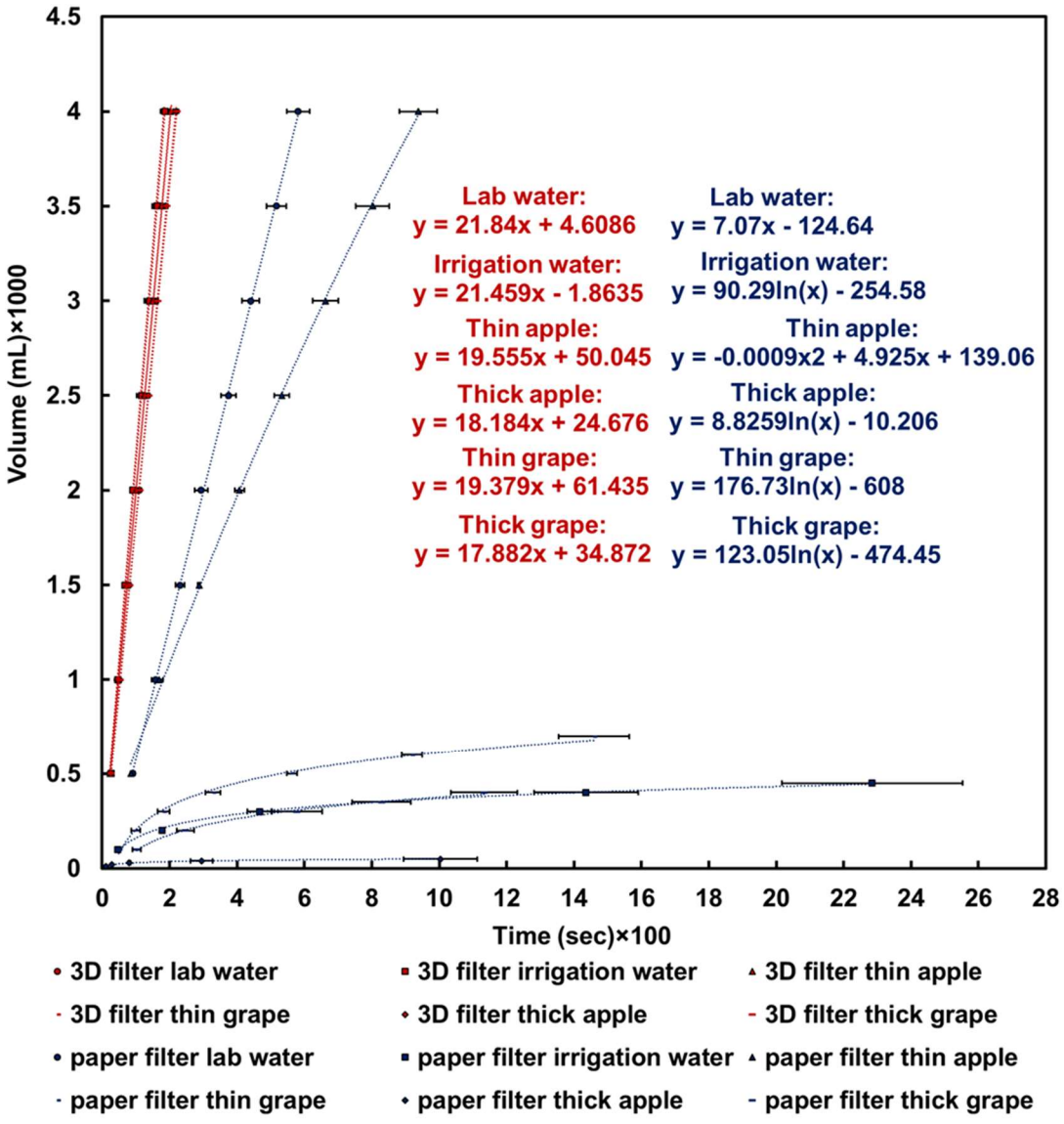


Figure 6. 11 Flow volume as a function of flow time by the 3D filter pipe system with 5,000 ME filter elements aligned in it and the vacuumed-paper filter system.

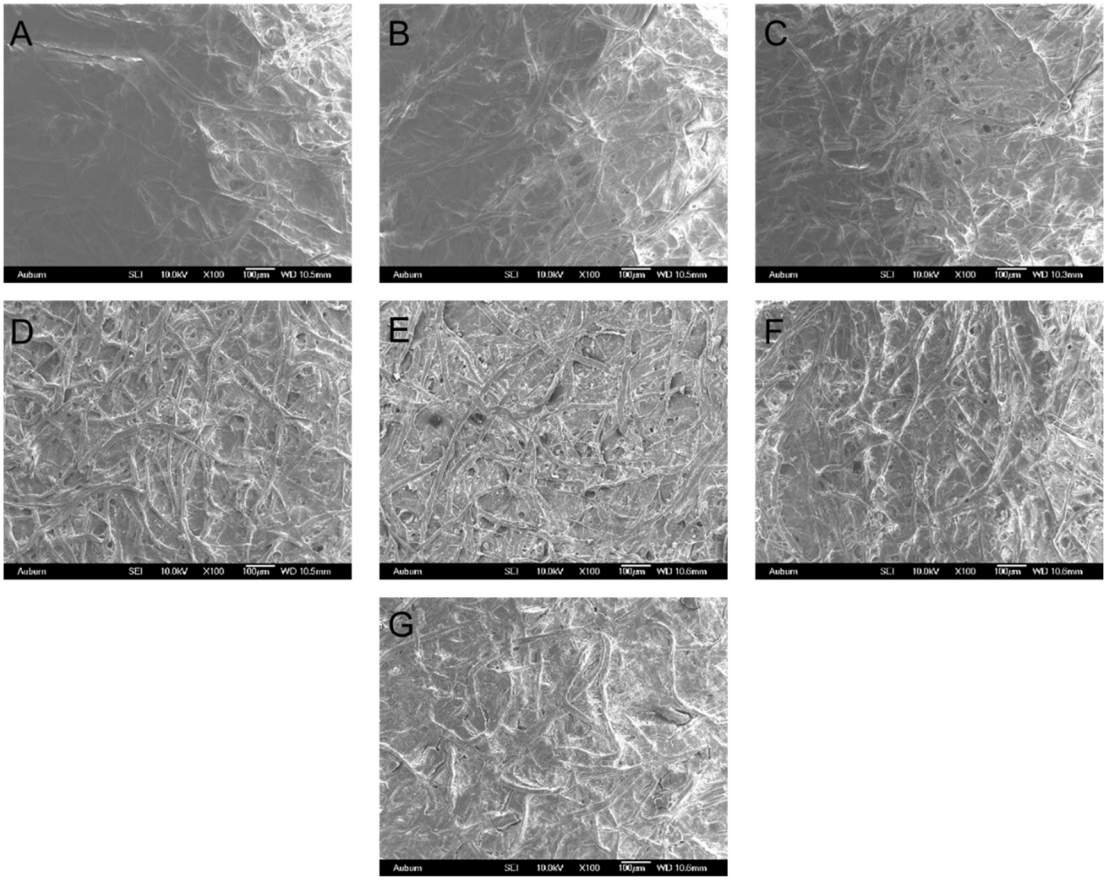


Figure 6. 12 SEM image of micro-surfaces on filter papers passed by lab water (B), thin apple juice (C), irrigation water (D), thin grape juice (E), thick apple juice (F), thick grape juice (G), and clean filter paper as reference (A).

### 6.3.3. Pathogen filtering performance with the number of ME filter elements

#### 6.3.3.1. Material and methods

The preparation of ME filter elements was the same as the previous experiment (Fabrication, E2 phage immobilization, and super blocking), except the size of 4 mm×0.8 mm×0.03 mm.

*Salmonella* suspensions were cultured in LB broth and prepared as described in the previous paper to the concentration of $5\times10^8$ cfu/mL (Sorokulova et al. 2005). Then, the stock *Salmonella* suspensions were further diluted to $5\times10^3$ cfu/mL. The *Salmonella* testing

suspensions of 20 mL with a concentration of 83 cfu/mL were prepared and ready to use by adding 0.33 mL of diluted *Salmonella* suspensions.

In the experiment, the filtering performance as a function of the number of ME filter elements was explored in the 20 mL *Salmonella* suspensions by the 8mm 3D filter system. The different numbers (5, 10, 20, 50, 75, 100, 125, 150, 200, 270, 370, 500, and 1,000) of 4 mm ME filter elements were aligned in the 8mm 3D filter pipe system by the uniform magnetic field, respectively. The *Salmonella* suspensions were passed through the 3D filter pipe system from the top inlet to the bottom outlet by gravity with the flow rate of 3 mm/s once. To reduce the consumption of ME filter elements, the *Salmonella* suspensions were circulated through the 8 mm 3D filter pipe system with 5,000 ME filter elements ten times, which was expected to be equivalent to the multi-fold number of 5,000 ME filter elements. After the sample loading, the same plate count method was applied to calculate the capture rates of the 3D filter with the different number of ME filter elements. For the circulation flow of *Salmonella* suspensions, the cyclic times ($2^{nd}$, $6^{th}$, and $10^{th}$) were selected to calculate the capture rates for the equivalent number (10,000, 30,000, and 50,000) of ME filter elements.

Moreover, Ansys Workbench Fluent software was also applied to simulate the flow condition of flow domain and the capture rate by the same method described in the previous chapter, excluding the turbulent length scale of 0.8 mm.

6.3.3.2. Results and discussion

The increased capture rate with the number of ME filter elements and the cyclic times of *Salmonella* suspensions are displayed in Figure 6.13. The increased capture rate was attributed to the increased number of ME filter elements and turbulence in the pipe system,

resulting in more binding sites and the higher binding possibility of *Salmonella* cells to the immobilized E2 phage. In the circulation flow of *Salmonella* suspensions, more binding opportunities of *Salmonella* cells were repeatedly provided by a certain amount of phage-immobilized ME filter elements and the turbulence produced in the filter pipe system. As more than thousands of binding sites are supplied by each E2 phage, the *Salmonella* cells can be captured by free binding sites in the circulation flow. Meanwhile, the bound *Salmonella* cells and *Salmonella*-phage complexes were also detached in the circulation flow, due to the physical adsorption of E2 phage. Despite the detachment performance, the capture rate was still increased. The increased capture rate resulted from the effective capture performance with a certain amount of ME filter elements in the circulation flow that the binding possibility was higher than the detaching chance. Transferring the cyclic times to the equivalent number of ME filter elements, the capture rate was combined with the number of ME filter elements in Figure 6.14. The increased capture rate was displayed with the natural logarithmic growth of the number of ME filter elements.

To further understand the effects of flow conditions on pathogen capture performance of the 3D filter system, the finite element analysis on turbulent kinetic energy and capture rate was conducted in a simulated liquid sample loading process. In the simulation, the turbulence in the liquid stream was produced in the 3D filter pipe system due to the aligned ME filter elements in it. The particles, similarly with the number of *Salmonella* cells, were mixed in the liquid stream and injected into the filter pipe system to explore the simulated capture rate.

As described in the previous subchapter, a cross-section plane along with the flow direction and the surfaces of ME filter elements were selected to create contour plots of

turbulence distribution in Figure 6.15A-B. The turbulence distribution with the different numbers (100, 200, 370, 500, and 1,000) of ME filter elements in the 3D filter system was plotted in Figure 6.15A, respectively, and the contour of turbulence distribution on the part of ME filter elements' surfaces is shown in Figure 6.15B. According to the turbulence distribution, the turbulent intensity was affected by the aligned ME filter elements in the filter pipe system. The low turbulent intensity was displayed in the flow area without ME filter elements. In contrast, the flow area, coupled with ME filter elements, was marked by the high turbulent intensity in red color. Furthermore, the turbulence distribution shown in Figure 6.15B was affected by the 3D structure of aligned ME filter elements, showing the color changed from blue to red on the surfaces of ME filter elements. In Figure 6.15C, the turbulent kinetic energy of the created plane and the full flow domain is displayed. The turbulent kinetic energy increased with an increase in the number of ME filter elements, resulting in the decreased flow rate and the increased contacting chance between *Salmonella* cells and E2 phage, which were two key factors to increase the capture possibility for ME filter elements.

Moreover, the comparison of capture rates between experiment and simulation in the 8 mm 3D filter system is plotted in Figure 6.16. The increasing tendency of the two fitting functions of experiment and simulation was consistent with the results in the initial 3D filter system. As shown in Figure 6.16, the steeper slope of fitting function for the simulation was achieved compared with the slope for the experiment. This difference between the two slopes can also be explained by the different capture mechanisms described in the initial 3D filter system. In the simulation of the 3D filter system, there was no weak interaction of physical adsorption between E2 phage and ME filter elements. All

trapped particles were calculated into the simulated capture rate. Different from the simulation, the actually captured *Salmonella* cells in the experiment decreased, due to the detachment of bound *Salmonella* cells and *Salmonella*-phage complexes.

Therefore, the capture and filtration performance of *Salmonella* pathogens from large volume of liquid streams have been demonstrated by the large-scale 3D filter system with the number of ME filter elements. The capture rate increased with an increase in the number of ME filter elements.

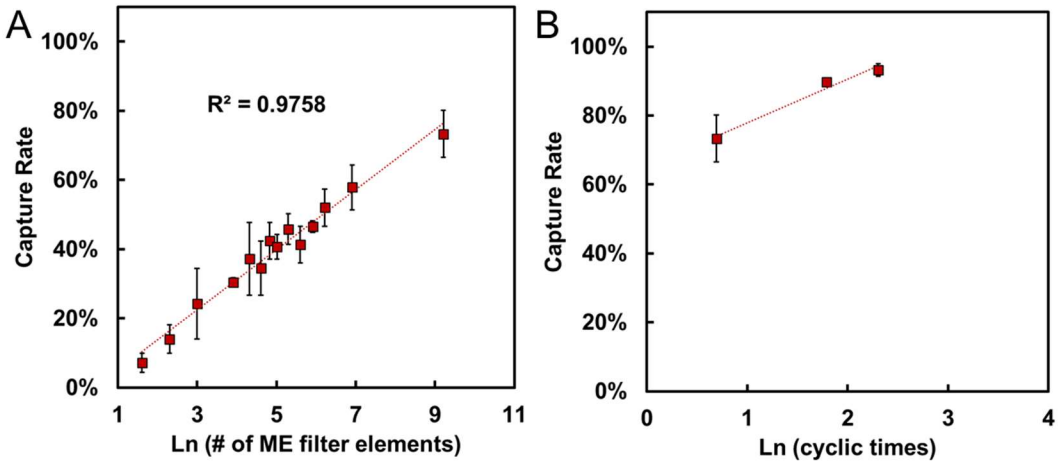


Figure 6. 13 Capture rate as a function of (a) the number of ME filter elements and (b) the cyclic times for liquid streams passed through.

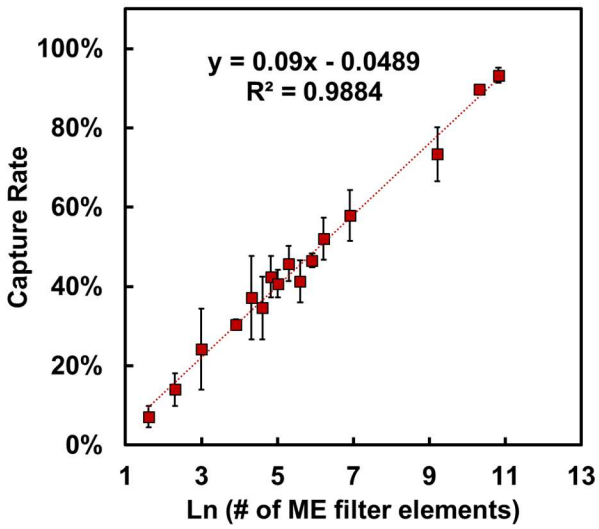


Figure 6. 14 Combined capture rate as a function of the number of ME filter elements.

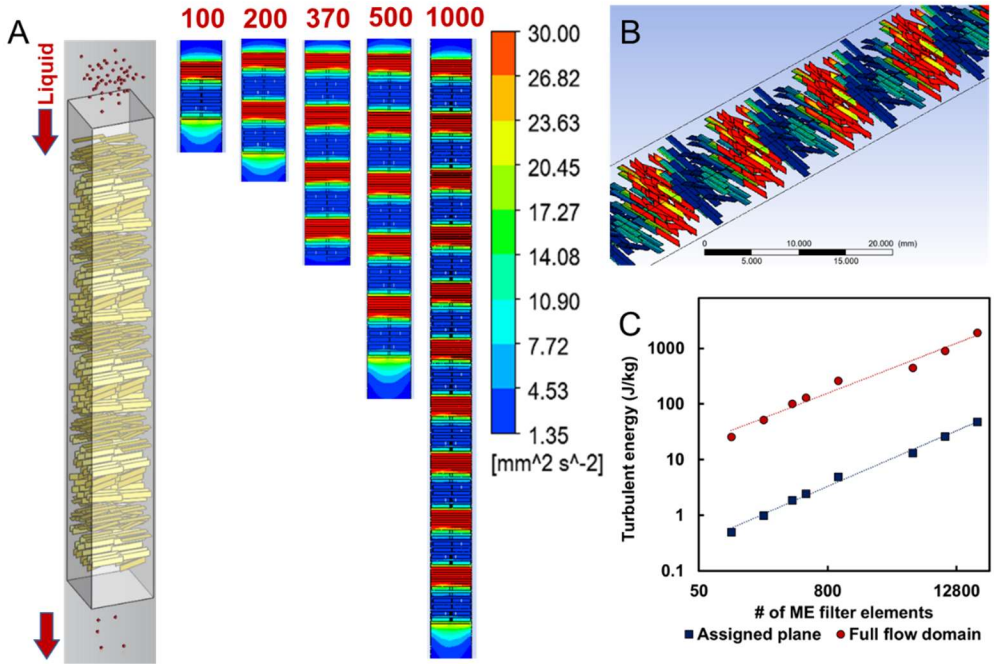


Figure 6. 15 (A) Particles as the substitute of pathogens with liquid stream were injected from the inlet of the 3D filter pipe system with aligned ME filter elements. Turbulence distribution was plotted on the created plan of flow liquid with the different number of ME filter elements. (B) Contour plot of the turbulence distribution on the 3D structure of partial ME filter elements' surfaces. (C) Total turbulent kinetic energy of the created plane and

full flow domain in the pipe system as a function of an increased number of ME filter elements.

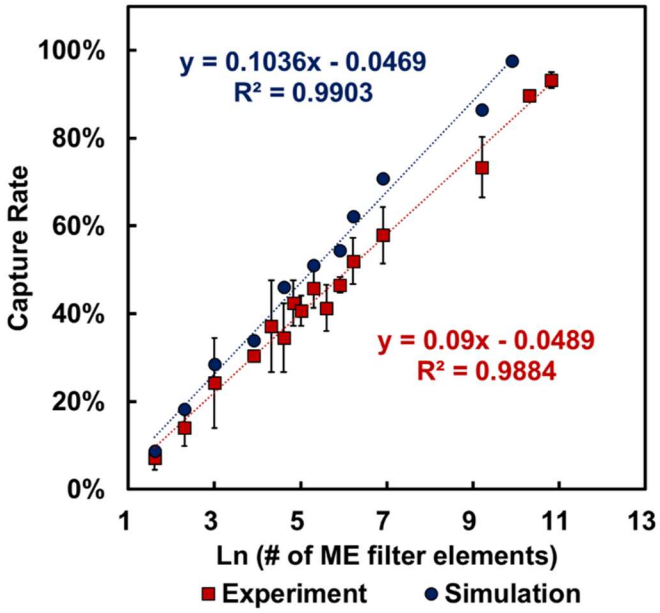


Figure 6. 16 Capture rate as a function of the number of ME filter elements in experiment and simulation.

### 6.3.4. Pathogen filtering performance with total surface area of ME filter elements

#### 6.3.4.1. Material and methods

The preparation of ME filter elements was the same as the previous experiment (Fabrication, E2 phage immobilization, and super blocking), excluding the sizes of 4 mm×0.8 mm×0.03 mm and 8 mm×1.6 mm×0.03 mm.

*Salmonella* suspensions were cultured in LB broth and prepared as described in the previous paper to the concentration of $5\times10^8$ cfu/mL (Sorokulova et al. 2005). Then, the stock *Salmonella* suspensions were further diluted to $5\times10^3$ cfu/mL. 40 mL *Salmonella* testing suspensions with the same concentration of 83 cfu/mL were prepared with DI water and 0.66 mL of diluted *Salmonella* suspensions.

In the experiment, the filtering performance with the total surface area of ME filter elements was explored in the 40 mL *Salmonella* suspensions by the 16 mm 3D filter pipe system. The different numbers of 4 mm and 8 mm ME filter elements were aligned in the 16 mm 3D filter pipe system by the uniform magnetic field, respectively. The 40 mL *Salmonella* suspensions were passed through the 3D filter pipe system from the top inlet to the bottom outlet by gravity with the flow rate of 3 mm/s once. To reduce the consumption of ME filter elements, the *Salmonella* suspensions were circulated through the 16 mm 3D filter pipe system multiple times, which might be equivalent to the multi-fold number of ME filter elements. For the 2,000, 5000, 10,000, and 20,000 of 4 mm ME filter elements, the *Salmonella* suspensions were circulated 10, 10, 15, and 25 times, respectively. For the 1,000 and 10,000 of 8 mm ME filter elements, the *Salmonella* suspensions were circulated 15 and 20 times, respectively. After the sample loading, the same plate count method was applied to calculate the capture rates for the different numbers of ME filter elements.

Moreover, the turbulent kinetic energy for the 16 mm 3D filter pipe system with the different numbers of 4 mm & 8 mm ME filter elements was simulated by Ansys Workbench Fluent software. The same method described in the previous chapter was used, excluding the turbulent length scale of 2 mm. As the limitation of CPU and memory, several numbers of ME filter elements (370, 2,000, 5,000, and 8,000 of 4 mm ME filter elements, 5,000 and 10,000 of 8 mm ME filter elements) were selected.

#### 6.3.4.2. Results and discussion

The pathogen filtering performance with the total surface area of ME filter elements was explored by the 16 mm 3D filter pipe system with 4 mm & 8 mm ME filter elements.

Directly transferring the cyclic times to the equivalent number of ME filter elements, the capture rate as a function of the number of 4 mm & 8 mm ME filter elements is displayed in Figure 6.17. As shown in Figure 6.17, the capture rate increased with an increased natural logarithmic value of the number of 4 mm & 8 mm ME filter elements, respectively. More than 90% capture rate was achieved for both 4 mm and 8 mm ME filter elements. From Figure 6.17, the less number of 8 mm ME filter elements were needed to obtain the same capture rate, compared with the number of 4 mm ME filter elements. The result is anticipated to be affected by the total surface area of ME filter elements since the total surface area is the only variable in the experiment. With increasing the total surface area for the same number of ME filter elements, the turbulence was increased due to the larger influential region in the liquid stream. As discussed in the previous subchapter, the decreased instant flow velocity between the gaps of ME filter elements and the more contacting chance between *Salmonella* pathogens and ME filter elements in the testing suspensions were formed by turbulence, resulting in the higher capture possibility. The increased capture rate was expected to be provided with the increased turbulence produced from the larger surface area of 8 mm ME filter elements. This anticipation is verified by the turbulent kinetic energy in the finite element analysis. The total surface area of ME filter elements was calculated from the number of ME filter elements and the unit area (4 mm×0.8 mm & 8 mm×1.6 mm) of ME filter elements, respectively. The increased turbulent kinetic energy is displayed with a linear increase in the total surface area of ME filter elements in Figure 6.18. Hence, the decreased flow velocity of the *Salmonella* suspensions and the more contacting chance between *Salmonella* pathogens and ME filter

elements, which are produced from the increased turbulence, are the two key factors to increase the capture possibility for ME filter elements.

Furthermore, by transferring the number of 4 mm & 8 mm ME filter elements to the total surface area, the capture rate displayed in Figure 6.17 was normalized with the total surface area of ME filter elements, as shown in Figure 6.19. The linearly increased capture rate was presented with a natural logarithmic value of the increased total surface area of ME filter elements. Therefore, the pathogen capture and filtration performance of the 3D filter 2.0 system as a function of the total surface area of ME filter elements is demonstrated.

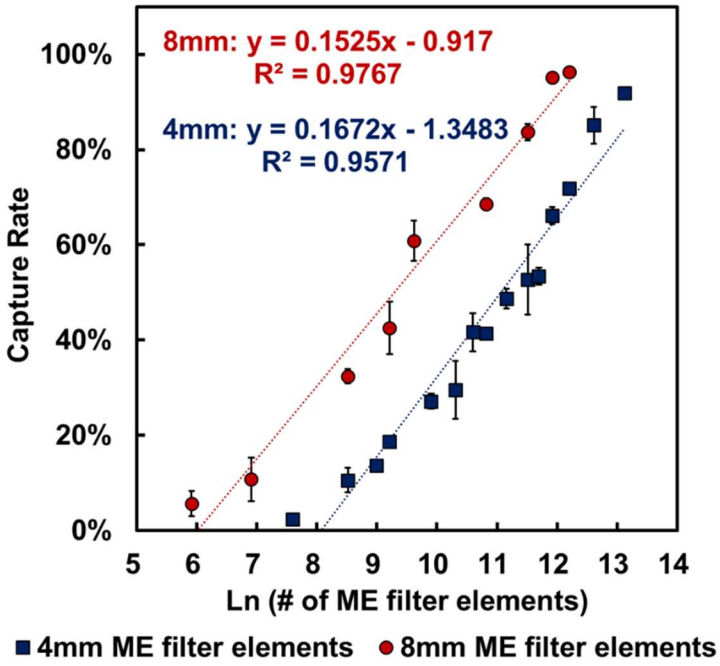


Figure 6. 17 Capture rate as a function of the number of 4mm & 8mm ME filter elements in 16 mm 3D filter pipe system.

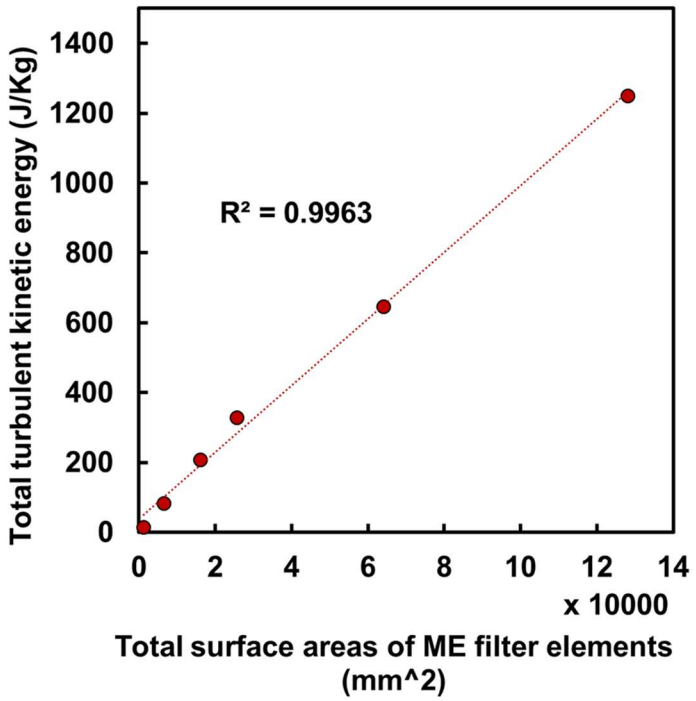


Figure 6. 18 Turbulent kinetic energy as a function of the total surface area of ME filter elements in 16 mm 3D filter pipe system.

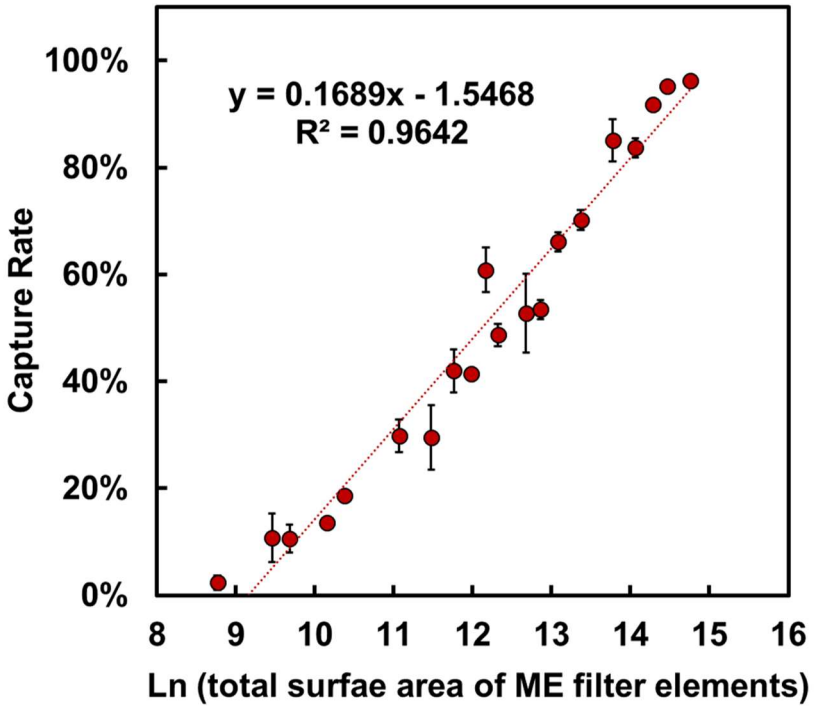


Figure 6. 19 Capture rate as a function of the total surface area of ME filter elements.

## 6.4. Multipipe-3D filter 2.0

### 6.4.1. Introduction

Based on the success of *Salmonella* pathogens filtration from large volume of pathogen suspensions in the large-scale-3D filter system with ME filter elements, a multipipe-3D filter system was developed to investigate the filtering performance with increased volume of pathogen suspensions. The increased volume of pathogen suspensions was passed through the multipipe-3D filter system simultaneously to keep the same flow time. Compared with the same volume of liquid streams passed through the single pipe of 3D filter system, the flow time was economized in the multipipe-3D filter system. In this experiment, the multipipe-3D filter consisted of 4 mm ME filter elements per pipe, the pair of uniform magnetic plates, and the multipipe-3D filter pipe system. The multipipe-3D filter pipe systems were constructed by bound-8 mm square glass pipes and a shared valve in Figure 6.20, including single-pipe, two-pipes, three-pipes, four-pipes, and six-pipes. In this subchapter, the capturing and filtering performance of the multipipe-3D filter system were tested by different volumes of pathogen suspensions. The filtering performance for the different volumes of pathogen suspensions was normalized to discuss the interaction between the volume and the cyclic times of pathogen suspensions in the multipipe-3D filter system.

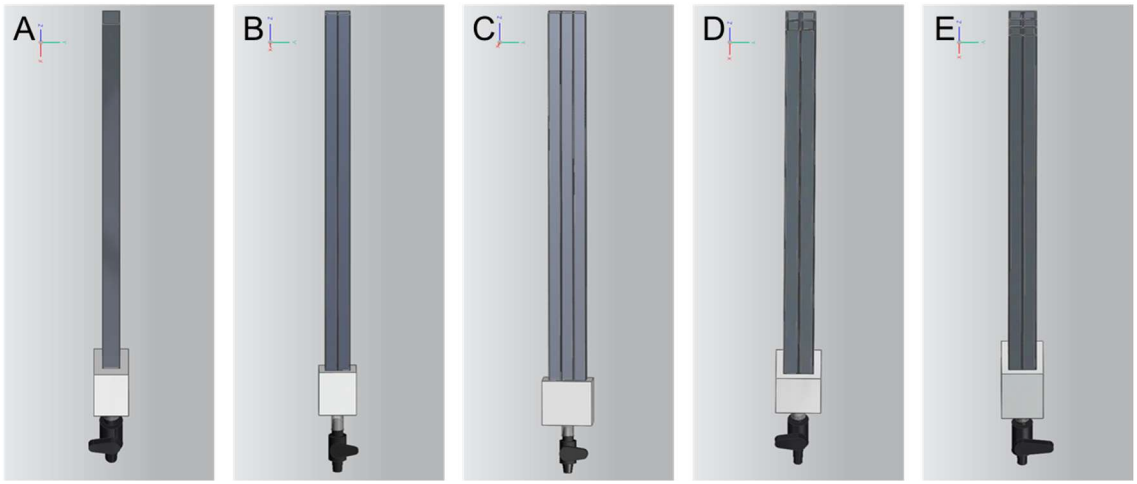


Figure 6. 20 Multipipe-3D filter pipe systems: (A) Single-pipe; (B) Two-pipes; (C) Three-pipes; (D) Four-pipes; (E) Six-pipes.

### 6.4.2. Material and methods

The preparation of ME filter elements was the same as the previous experiment (Fabrication, E2 phage immobilization, and super blocking), excluding the size of 4 mm× 0.8 mm×0.03 mm.

*Salmonella* suspensions were cultured in LB broth and prepared as described in the previous paper to the concentration of $5\times10^8$ cfu/mL (Sorokulova et al. 2005). The stock *Salmonella* suspensions were further diluted to $5\times10^3$ cfu/mL. 0.66 mL, 0.99 mL, 1.32 mL, and 1.98 mL of diluted *Salmonella* suspensions with the concentration of $5\times10^3$cfu/ml were mixed with DI water to prepare 40 mL, 60 mL, 80 mL, and 120 mL *Salmonella* suspensions with the same concentration of 83 cfu/mL, respectively. As the single-pipe-3D filter system has been tested in the previous subchapter, the experimental data can be used directly.

In this experiment, the filtering performance with increased volume of *Salmonella* suspensions was explored by the multipipe-3D filter pipe systems with 4 mm ME filter elements aligned in them. The different numbers of 4 mm ME filter elements were aligned

in each pipe of the multipipe-3D filter pipe systems, respectively. The *Salmonella* suspensions (40 mL, 60 mL, 80 mL, and 120 mL) were passed through the multipipe-3D filter systems (two-pipes, three-pipes, four-pipes, and six-pipes) from the top inlet to the bottom outlet with the flow rate of 3 mm/s once, respectively. For the consumption of more than 5,000 ME filter elements in each pipe, the circulation flow of *Salmonella* suspensions was still selected to use in the multipipe-3D filter system. The circulation flow of *Salmonella* suspensions in the multiple-3D filter pipe system with 5,000 ME filter elements was expected to be equivalent to the multi-fold number of 5,000 ME filter elements. The *Salmonella* suspensions were circulated 20 times for the two-pipes, three-pipes, and four-pipes-3D filter systems, respectively, and 40 times for the six pipes-3D filter system. After the sample loading, the same plate count method was applied to calculate the capture rates for the different numbers of ME filter elements. For the circulation flow of *Salmonella* suspensions, the cyclic times ($1^{st}$, $4^{th}$, $6^{th}$, $10^{th}$, $15^{th}$, and $20^{th}$) for two-pipes, three-pipes, and four-pipes-3D filter systems and the cyclic times ($1^{st}$, $6^{th}$, $10^{th}$, $15^{th}$, $20^{th}$, $30^{th}$, and $40^{th}$) for six-pipes-3D filter system were selected to calculate the capture rates for the equivalent number of ME filter elements.

### 6.4.3. Results and discussion

In the subchapter, the filtering performance with the increased volume of *Salmonella* suspensions was tested by the multipipe-3D filter system. The increased capture rate is displayed in Figure 6.21 with a natural logarithmic number of ME filter elements and the cyclic times of *Salmonella* suspensions. As discussed in the previous subchapter, the increased capture rate with the number of ME filter elements resulted from the increased contacting chance of *Salmonella* cells to the E2 phage due to the increased turbulence. In

the circulation flow of *Salmonella* suspensions, more binding opportunities were provided by a certain amount of ME filter elements and the turbulence, when the binding possibility was higher than the detaching chance. Transferring the cyclic times to the equivalent number of ME filter elements, the capture rate was combined with the equivalent number of ME filter elements in Figure 6.22. The increased capture rate is displayed with the natural logarithmic growth of the number of ME filter elements in the multipipe-3D filter systems. More than 90% capture rate could be achieved by the multipipe-3D filter system. The filtration of *Salmonella* pathogens from the increased volume of liquids is demonstrated by increasing the number of pipes in the 3D filter system, even though the fitting function was shifted down gradually. However, the same filtering mechanism of the multipipe-3D filter system was demonstrated by the similar slopes of five fitting functions.

Based on the same capture mechanism of the multipipe-3D filter system, the five fitting functions of capture rate were integrated and normalized. The natural logarithmic value of the equivalent number of 4 mm ME filter elements per pipe to achieve 90% capture rate was calculated for the different volumes of *Salmonella* suspensions by the fitting functions, as shown in Table 6.2. The natural logarithmic values for the cyclic times of *Salmonella* suspensions shown in Table 6.2 were calculated by the operational rule of natural logarithm shown in equation 6.1. The increased natural logarithmic values of the cyclic times are displayed in Figure 6.23, with increasing the volume of *Salmonella* suspensions. Depending on the fitting function in Figure 6.23, cyclic times for *Salmonella* suspensions can be calculated with the volume range from 20 mL to 120 mL. Beyond the volume range, this fitting function can be a reference to estimate cyclic times for a specific volume of *Salmonella* suspensions.

Therefore, the filtration of *Salmonella* pathogens from increased volume of *Salmonella* suspensions is demonstrated by the multipipe-3D filter systems with 4 mm ME filter elements. The multipipe-3D filter pipe system can be used for the filtration of increased volume of pathogen suspensions. The theoretical interaction between the cyclic times and the volume range from 20 mL to 120 mL can be a reference to estimate the cyclic times for a specific volume of pathogen suspensions.

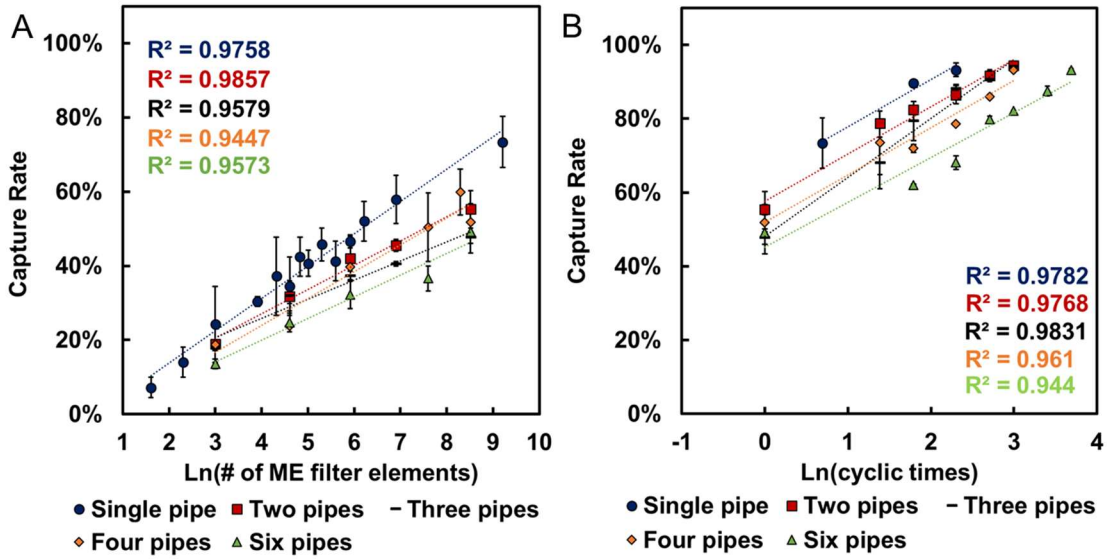


Figure 6. 21 Capture rate as a function of: (A) the number of ME filter elements; (B) the number of cyclic times for *Salmonella* suspensions in the multipipe-3D filter systems.

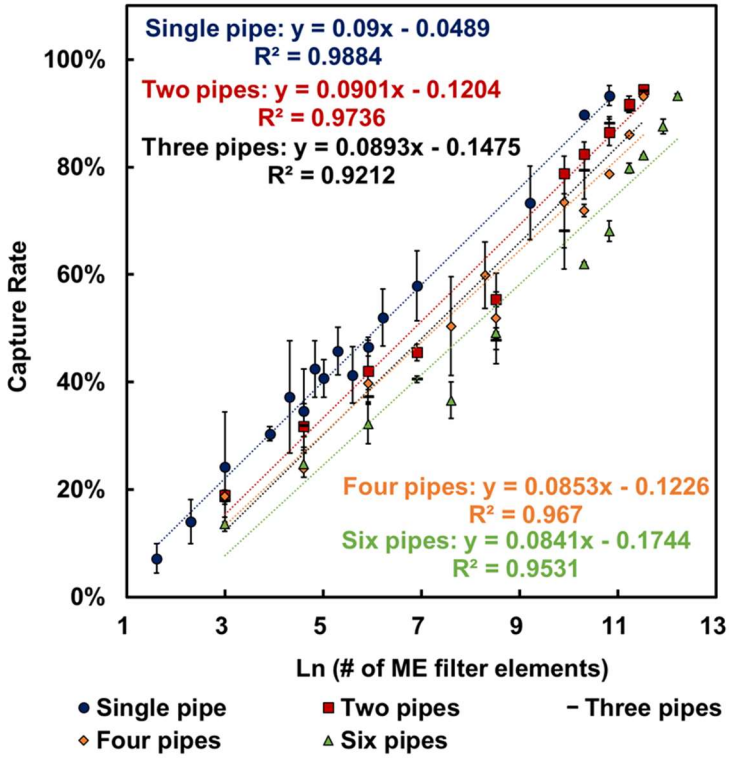


Figure 6. 22 Combined capture rate as a function of the equivalent number of ME filter elements for the multipipe-3D filter systems.

$$Ln(cyclic\ times) = Ln(\#\ of\ ME\ filter\ elements) - Ln(5,000) \qquad \text{Equation 6. 1}$$

Table 6. 1 The calculated natural logarithmic value of the number of ME filter elements and the cyclic times of *Salmonella* suspensions for 90% filtration of *Salmonella* pathogens.

| Volume (mL) | Ln (# of ME filter elements) | Ln (cyclic times) |
|---|---|---|
| 20 | 10.54 | 2.03 |
| 40 | 11.33 | 2.81 |
| 60 | 11.73 | 3.21 |
| 80 | 11.99 | 3.47 |
| 120 | 12.78 | 4.26 |

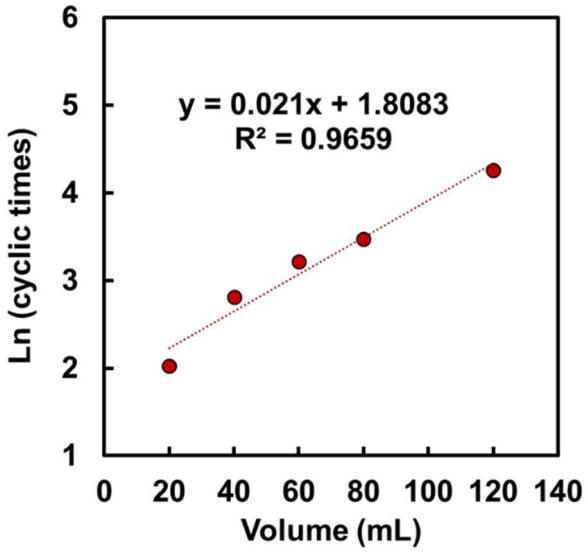


Figure 6. 23 Cyclic times of *Salmonella* suspensions as a function of volume in the multipipe-3D filter systems.

### 6.5. Conclusions

In this chapter, the capture and filtration of *Salmonella* pathogens from *Salmonella* suspensions were demonstrated by the 3D filter 2.0 system. The anti-clogging and high throughput experiments illustrated that large volume of liquids could pass through the anti-clogging 3D filter 2.0 system with high throughput. The capture rate of more than 90% was achieved by the 3D filter 2.0 system with increasing the number and the total surface area of ME filter elements. In the 3D filter 2.0 system, the turbulence, created by ME filter elements, was the key factor in providing decreased flow velocity and more contacting chance of *Salmonella* cells captured by E2 phage in the *Salmonella* suspensions. The turbulent kinetic energy increased with increasing the number and the total surface area of ME filter elements. Besides the development of single-pipe-3D filter 2.0 systems, multipipe-3D filter 2.0 systems with circulation flow were explored to realize the filtration of *Salmonella* pathogens from the increased volume of *Salmonella* suspensions. Based on

that, the interaction between the volume and the cyclic times of *Salmonella* suspensions to achieve the 90% capture rate could be a reference to estimate cyclic times for a specific volume of pathogen suspensions in the multipipe-3D filter system.

Chapter 7

## 7. Conclusions and future work

In the dissertation, a new technology, 3D phage-based biomolecular filter, was developed to rapidly capture and concentrate foodborne pathogens from large volume of liquid streams. The 3D filter consisted of the phage-immobilized ME filter elements, the magnetic field, and the 3D filter pipe system. Multiple ME resonators with immobilized E2 phage were served as ME filter elements. The magnetic field was created by electromagnetic solenoid coils or permanent magnets. The ME filter elements aligned by the magnetic field were employed to capture and concentrate foodborne pathogens from large volume of liquid streams in the 3D filter system. Two versions of the 3D filter system in the research were developed. The 3D filter 1.0 system consisted of ME filter elements, electromagnetic supporting frames, and a 3D filter 1.0 pipe system. The frameless 3D filter 2.0 system was constructed by ME filter elements, a pair of permanent magnetic plates, and a 3D filter 2.0 pipe system.

In the 3D filter 1.0 system, the electromagnetic field produced by the solenoid coils was conducted to align ME filter elements on supporting frames. The designed structure of supporting frames was verified by simulation of the magnetic field flux vector. From the commercial market, the soft magnetic material, Permalloy 80 alloy, was selected to fabricate the supporting frames. The temperature variation test illustrated that the *Salmonella* pathogens in suspensions and the robustness of E2 phage were not affected by the heat produced by the solenoid coils in 10mins. For the 3D filter 1.0 system, the capture rate increased with an increase in the number of filter layers. However, the low capture rate

and the density of aligned ME filter elements were required to be improved, resulting in the development of the frameless 3D filter 2.0 system.

Due to the failure of filtration by the 3D filter 1.0 system, the filtering capability of ME filter elements for *Salmonella* pathogens from the small volume of *Salmonella* suspensions was explored by the 2D filter system, followed by the development of 3D filter 2.0 system. The filtration of *Salmonella* pathogens from *Salmonella* suspensions was demonstrated by the 2D filter experiment.

Based on the experiment of 2D filter, the 3D filter 2.0 system was developed. A pair of permanent magnetic plates were used to supply the uniform magnetic field to align ME filter elements, instead of the electromagnetic solenoid coils, in the 3D filter 2.0 system. To compare with the capturing and filtering performance of the 2D filter, the initial 3D filter 2.0 pipe system with 1 mm ME filter elements was developed. The filtration of *Salmonella* pathogens from *Salmonella* suspensions and the turbulent flow condition were explored by experiment and finite element analysis. And then, the large-scale-3D filter 2.0 system was constructed to study the anti-clogging characteristic, high throughput performance, and filtering performance with the number and total surface area of ME filter elements. The anti-clogging characteristic and high throughput performance were demonstrated by the large-scale 3D filter 2.0 system. The finite element analysis and the experiments about the large-scale 3D filter 2.0 system were conducted to explore the turbulent flow condition of liquids and the filtering performance with the number and the total surface area of ME filter elements. Besides the single-pipe 3D filter 2.0 system, the multipipe-3D filter 2.0 system was developed to explore the filtering performance of *Salmonella* pathogens from increased volume of *Salmonella* suspensions. The interaction

between volumes and the cyclic times of *Salmonella* suspensions was investigated by the multipipe-3D filter 2.0 system with circulation flow to achieve 90% filtration, which could be a reference to design the multipipe-3D filter 2.0 system for a specific volume of pathogen suspensions.

For the exploration of capturing and filtering performance of *Salmonella* pathogens from large volume of liquid streams by the 3D phage-based biomolecular filter system, the following conclusions are listed:

1. Capture rate of the 3D filter 1.0 system increased with increasing the number of filter layers. But the low capture rate was displayed;
2. Filtration of *Salmonella* pathogens in small volume of *Salmonella* suspensions was demonstrated by the 2D filter system with increasing the number of ME filter elements;
3. Anti-clogging characteristic and high throughput performance of the 3D filter 2.0 system were demonstrated;
4. Filtration of *Salmonella* pathogens from large volume of liquid streams was realized by the large-scale-3D filter 2.0 system, where the capture rate increased with increasing the number and total surface area of ME filter elements;
5. The increased contacting chance and the decreased flow velocity in liquid stream, produced by the increased turbulence, were two key factors to increase the capture probability, resulting from the increased number and total surface area of ME filter elements.
6. Filtration of *Salmonella* pathogens from increased volume of liquid streams was demonstrated by the multipipe-3D filter 2.0 system with circulation flow. The

normalized interaction between the cyclic times and the volumes of liquid streams can be a reference to estimate cyclic times for a specific volume of pathogen suspensions to achieve a 90% filtration.

Hence, the anti-clogging 3D phage-based biomolecular filter is a new method to capture and concentrate foodborne pathogens from large volume of liquid streams with high throughput.

In future work, several plans are listed as followed:

1. Besides the *Salmonella typhimurium* pathogens, other foodborne pathogens will be detected by the 3D phage-based biomolecular filter 2.0 system, such as *E. coli*;
2. Besides the DI water, other liquids will be tested to investigate the filtering performance of the 3D phage-based biomolecular filter 2.0 system, such as tap water, irrigation water, and juices;
3. The filtration of pathogens from larger volume of pathogen suspensions will be investigated by the multipipe-3D phage-based biomolecular filter 2.0 system with more pipes;
4. An automated, integrated cell counter with laser sources and detectors will be developed to count target pathogens.

## References

Abdel-Hamid, Ihab, Dmitri Ivnitski, Plamen Atanasov, and Ebtisam Wilkins. 1999a. "Flow-through Immunofiltration Assay System for Rapid Detection of E. Coli O157:H7." *Biosensors and Bioelectronics*. https://doi.org/10.1016/S0956-5663(99)00004-4.

Abdel-Hamid, Ihab, Dmitri Ivnitski, Plamen Atanasov, and Ebtisam Wilkins. 1999b. "Highly Sensitive Flow-Injection Immunoassay System for Rapid Detection of Bacteria." *Analytica Chimica Acta*. https://doi.org/10.1016/S0003-2670(99)00580-2.

Al-Holy, Murad A., Mengshi Lin, Anna G. Cavinato, and Barbara A. Rasco. 2006. "The Use of Fourier Transform Infrared Spectroscopy to Differentiate Escherichia Coli O157:H7 from Other Bacteria Inoculated into Apple Juice." *Food Microbiology* 23 (2): 162–68. https://doi.org/10.1016/j.fm.2005.01.017.

Alahi, Md Eshrat E., and Subhas Chandra Mukhopadhyay. 2017. "Detection Methodologies for Pathogen and Toxins: A Review." *Sensors (Switzerland)* 17 (8): 1–20. https://doi.org/10.3390/s17081885.

Alexander A. Gall, Igor V. Kutyavin, Nicolaas M. J. Vermeulen, Robert O. Dempcy. 2003. Non-aggregating, non-quenching oligomers comprising nucleotide analogues; methods of synthesis and use thereof, issued 2003.

Amjed Abdullah, Shibajyoti Ghosh Dastider, Ibrahem Jasim1, Zhenyu Shen, Nuh Yuksek, Shuping Zhang, Majed Dweik, Mahmoud Almasri. 2019. "Microfluidic Based Impedance Biosensor for Pathogens Detection in Food Products." *Electrophoresis* 40: 508–20.

Banerjee, Pratik, Dominik Lenz, Joseph Paul Robinson, Jenna L. Rickus, and Arun K. Bhunia. 2008. "A Novel and Simple Cell-Based Detection System with a Collagen-Encapsulated B-Lymphocyte Cell Line as a Biosensor for Rapid Detection of Pathogens and Toxins." *Laboratory Investigation* 88 (2): 196–206. https://doi.org/10.1038/labinvest.3700703.

Berkenpas, E., P. Millard, and M. Pereira da Cunha. 2006. "Detection of Escherichia Coli O157:H7 with Langasite Pure Shear Horizontal Surface Acoustic Wave Sensors." *Biosensors and*

*Bioelectronics* 21 (12): 2255–62. https://doi.org/10.1016/j.bios.2005.11.005.

Bhunia, Arun K., Tao Geng, Amanda Lathrop, Angela Valadez, and Mark T. Morgan. 2004. "Optical Immunosensors for Detection of Listeria Monocytogenes and Salmonella Enteritidis from Food." *Monitoring Food Safety, Agriculture, and Plant Health* 5271 (March 2004): 1. https://doi.org/10.1117/12.515900.

Brogioni, Barbara, and Francesco Berti. 2014. "Surface Plasmon Resonance for the Characterization of Bacterial Polysaccharide Antigens: A Review." *MedChemComm* 5 (8): 1058–66. https://doi.org/10.1039/c4md00088a.

Cady, Nathaniel C., Scott Stelick, Madanagopal V. Kunnavakkam, and Carl A. Batt. 2005. "Real-Time PCR Detection of Listeria Monocytogenes Using an Integrated Microfluidics Platform." *Sensors and Actuators, B: Chemical* 107 (1 SPEC. ISS.): 332–41. https://doi.org/10.1016/j.snb.2004.10.022.

Carlyle CA, Svejcar M, et, Al. 2002. "A Cell-Based Biosensor Assay for Toxin Activity Detection of Bacterial Origin." In *The 102nd ASM General Meeting*, p369.

CDC. 2018a. "Bioterrorism Agents/Diseases." 2018. https://emergency.cdc.gov/agent/agentlist-category.asp.

CDC. 2018b. "CDC and Food Safety." 2018. https://www.cdc.gov/foodsafety/pdfs/CDC-Food-Safety-2018-H.pdf.

CDC. 2018c. "Outbreak of Salmonella Infections Linked to Hy-Vee Spring Pasta Salad." 2018. https://www.cdc.gov/salmonella/sandiego-07-18/index.html.

CDC. 2019a. "Antibiotic Resistance and Food Safety." 2019. https://www.cdc.gov/foodsafety/challenges/antibiotic-resistance.html.

CDC. 2019b. "Foodborne Illnesses and Germs." 2019. https://www.cdc.gov/foodsafety/foodborne-germs.html.

CDC. 2019c. "Outbreak of Salmonella Infections Linked to Pre-Cut Melons." 2019. https://www.cdc.gov/salmonella/carrau-04-19/index.html.

CDC. 2019d. “Salmonella.” 2019. https://www.cdc.gov/salmonella/index.html.

Chai, Yating. 2014. “Real-Time, in-Situ Detection of Pathogenic Bacteria on Food Surfaces Using a Surface-Scanning Coil Detector and Phage-Based Magnetoelastic Biosensors.” Auburn University.

Chai, Yating, Shin Horikawa, Suiqiong Li, Howard C. Wikle, and Bryan A. Chin. 2013. “A Surface-Scanning Coil Detector for Real-Time, in-Situ Detection of Bacteria on Fresh Food Surfaces.” *Biosensors and Bioelectronics* 50: 311–17. https://doi.org/10.1016/j.bios.2013.06.056.

Chai, Yating, Suiqiong Li, Shin Horikawa, Mi-Kyung Park, Vitaly VodyaNnoy, and A. Bryan Chin. 2012. “Rapid and Sensitive Detection of Salmonella Typhimurium on Eggshells by Using Wireless Biosensors.” *Journal of Food Protection* 75 (4): 631–36. https://doi.org/10.4315/0362-028x.jfp-11-339.

Chemburu, Sireesha, Ebtisam Wilkins, and Ihab Abdel-Hamid. 2005. “Detection of Pathogenic Bacteria in Food Samples Using Highly-Dispersed Carbon Particles.” *Biosensors and Bioelectronics* 21 (3): 491–99. https://doi.org/10.1016/j.bios.2004.11.025.

Chen, I. Hsuan, Shin Horikawa, Kayla Bryant, Rebecca Riggs, Bryan A. Chin, and James M. Barbaree. 2017. “Bacterial Assessment of Phage Magnetoelastic Sensors for Salmonella Enterica Typhimurium Detection in Chicken Meat.” *Food Control* 71: 273–78. https://doi.org/10.1016/j.foodcont.2016.07.003.

Chen, Sz Hau, Vivian C.H. Wu, Yao Chen Chuang, and Chih Sheng Lin. 2008. “Using Oligonucleotide-Functionalized Au Nanoparticles to Rapidly Detect Foodborne Pathogens on a Piezoelectric Biosensor.” *Journal of Microbiological Methods* 73 (1): 7–17. https://doi.org/10.1016/j.mimet.2008.01.004.

Crowley, Elizabeth L., Ciara K. O’Sullivan, and George G. Guilbault. 1999. “Increasing the Sensitivity of Listeria Monocytogenes Assays: Evaluation Using ELISA and Amperometic Detection.” *Analyst* 124 (3): 295–99. https://doi.org/10.1039/a806875e.

Dastider, Shibajyoti Ghosh, Syed Barizuddin, Nuh S. Yuksek, Majed Dweik, and Mahmoud

F. Almasri. 2015. “Efficient and Rapid Detection of Salmonella Using Microfluidic Impedance Based Sensing.” *Journal of Sensors* 2015. https://doi.org/10.1155/2015/293461.

Dong, Xiuli, and Liju Yang. 2015. “Dual Functional Nisin-Multi-Walled Carbon Nanotubes Coated Filters for Bacterial Capture and Inactivation.” *Journal of Biological Engineering* 9 (1): 1–11. https://doi.org/10.1186/s13036-015-0018-8.

Ercole, C., M. Del Gallo, L. Mosiello, S. Baccella, and A. Lepidi. 2003. “Escherichia Coli Detection in Vegetable Food by a Potentiometric Biosensor.” *Sensors and Actuators, B: Chemical* 91 (1–3): 163–68. https://doi.org/10.1016/S0925-4005(03)00083-2.

Fernandes, Ana C., Carla M. Duarte, Filipe A. Cardoso, Ricardo Bexiga, Susana Cardoso, and Paulo P. Freitas. 2014. “Lab-on-Chip Cytometry Based on Magnetoresistive Sensors for Bacteria Detection in Milk.” *Sensors (Switzerland)* 14 (8): 15496–524. https://doi.org/10.3390/s140815496.

Goeller, Lindsay J., and Mark R. Riley. 2007. “Discrimination of Bacteria and Bacteriophages by Raman Spectroscopy and Surface-Enhanced Raman Spectroscopy.” *Applied Spectroscopy* 61 (7): 679–85. https://doi.org/10.1366/000370207781393217.

Grimes, C. A., K. G. Ong, K. Loiselle, P. G. Stoyanov, D. Kouzoudis, Y. Liu, C. Tong, and F. Tefiku. 1999. “Magnetoelastic Sensors for Remote Query Environmental Monitoring.” *Smart Materials and Structures* 8 (5): 639–46. https://doi.org/10.1088/0964-1726/8/5/314.

Grow, Ann E., Laurie L. Wood, Johanna L. Claycomb, and Peggy A. Thompson. 2003. “New Biochip Technology for Label-Free Detection of Pathogens and Their Toxins.” *Journal of Microbiological Methods* 53 (2): 221–33. https://doi.org/10.1016/S0167-7012(03)00026-5.

Guntupalli, Rajesh, Ramji S. Lakshmanan, Michael L. Johnson, Jing Hu, Tung-Shi Huang, James M. Barbaree, Vitaly J. Vodyanoy, and Bryan A. Chin. 2007. “Magnetoelastic Biosensor for the Detection of Salmonella Typhimurium in Food Products.” *Sensing and Instrumentation for Food Quality and Safety* 1 (1): 3–10. https://doi.org/10.1007/s11694-006-9003-8.

Huang, Shichu, Suiqiong Li, Hong Yang, Michael L. Johnson, Jiehui Wan, I-Hsuan Chen, Valery A. Petrenko, James M. Barbaree, and Bryan A. Chin. 2008. “Optimization of Phage-Based

Magnetoelastic Biosensor Performance." *Sensor & Transducers Journal* 3: 87–96. http://www.sensorsportal.com/HTML/DIGEST/P_SI_59.htm.

Lazcka, Olivier, F. Javier Del Campo, and F. Xavier Muñoz. 2007. "Pathogen Detection: A Perspective of Traditional Methods and Biosensors." *Biosensors and Bioelectronics* 22 (7): 1205–17. https://doi.org/10.1016/j.bios.2006.06.036.

Lermo, A., S. Campoy, J. Barbé, S. Hernández, S. Alegret, and M. I. Pividori. 2007. "In Situ DNA Amplification with Magnetic Primers for the Electrochemical Detection of Food Pathogens." *Biosensors and Bioelectronics* 22 (9–10): 2010–17. https://doi.org/10.1016/j.bios.2006.08.048.

Maghari, Behrokh Mohajer, and Ali M. Ardekani. 2011. "Genetically Modified Foods and Social Concerns." *Avicenna Journal of Medical Biotechnology* 3 (3): 109–17.

Meeusen, C A, E C Alocilja, and W N Osburn. 2005. "Detection of E. Coli O157:H7 Using a Miniaturized Surface Plasmon Resonance Biosensor." *Transactions of the ASAE* 48 (6): 2409–16.

Meng, Jianghong, and Michael P. Doyle. 2002. "Introduction. Microbiological Food Safety." *Microbes and Infection* 4 (4): 395–97. https://doi.org/10.1016/S1286-4579(02)01552-6.

Millen, Hana T., Jordan C. Gonnering, Ryan K. Berg, Susan K. Spencer, William E. Jokela, John M. Pearce, Jackson S. Borchardt, and Mark A. Borchardt. 2012. "Glass Wool Filters for Concentrating Waterborne Viruses and Agricultural Zoonotic Pathogens." *Journal of Visualized Experiments*, no. 61: 6–11. https://doi.org/10.3791/3930.

Park, Mi Kyung, Suiqiong Li, and Bryan A et al. Chin. 2013. "Detection of Salmonella Typhimurium Grown Directly on Tomato Surface Using Phage-Based Magnetoelastic Biosensors." *Food and Bioprocess Technology* 6 (3): 682–89. https://doi.org/10.1007/s11947-011-0708-2.

Park, Mi Kyung, Jang Won Park, Howard C. Wikle, and Bryan A. Chin. 2013. "Evaluation of Phage-Based Magnetoelastic Biosensors for Direct Detection of Salmonella Typhimurium on Spinach Leaves." *Sensors and Actuators, B: Chemical* 176: 1134–40. https://doi.org/10.1016/j.snb.2012.10.084.

Petrenko, V. A., G. P. Smith, M. M. Mazooji, and T. Quinn. 2002. "A-Helically Constrained

Phage Display Library." *Protein Engineering* 15 (11): 943–50. https://doi.org/10.1093/protein/15.11.943.

Petrenko, Valery A. 2008. "Landscape Phage as a Molecular Recognition Interface for Detection Devices." *Microelectronics Journal* 39 (2): 202–7. https://doi.org/10.1016/j.mejo.2006.11.007.

Petrenko, Valery A., and Iryna B. Sorokulova. 2004. "Detection of Biological Threats. A Challenge for Directed Molecular Evolution." *Journal of Microbiological Methods* 58 (2): 147–68. https://doi.org/10.1016/j.mimet.2004.04.004.

Ruan, C, H Wang, and Y Li. 2002. "A Bienzyme Electrochemical Biosensor Coupled with Immunomagnetic Separation for Rapid Detection of Escherichia Coli O15:H7 in Food Samples." *Transactions of the ASAE* 45 (1): 249–55.

Salam, Faridah, Yildiz Uludag, and Ibtisam E. Tothill. 2013. "Real-Time and Sensitive Detection of Salmonella Typhimurium Using an Automated Quartz Crystal Microbalance (QCM) Instrument with Nanoparticles Amplification." *Talanta* 115: 761–67. https://doi.org/10.1016/j.talanta.2013.06.034.

Schmilovitch, Z, A Mizrach, V Alchanatis, G Kritzman, R Korotic, J Irudayaraj, and C Debroy. 2005. "Detection of Bacteria with Low-Resolution Raman Spectroscopy." *Transactions of the ASAE* 48 (5): 1843–50.

Singh, A., N. Glass, M. Tolba, L. Brovko, M. Griffiths, and S. Evoy. 2009. "Immobilization of Bacteriophages on Gold Surfaces for the Specific Capture of Pathogens." *Biosensors and Bioelectronics* 24 (12): 3645–51. https://doi.org/10.1016/j.bios.2009.05.028.

Sorokulova, Iryna B., Eric V. Olsen, I. Hsuan Chen, Ben Fiebor, James M. Barbaree, Vitaly J. Vodyanoy, Bryan A. Chin, and Valery A. Petrenko. 2005. "Landscape Phage Probes for Salmonella Typhimurium." *Journal of Microbiological Methods* 63 (1): 55–72. https://doi.org/10.1016/j.mimet.2005.02.019.

Stephen Ostroff, M.D. 2018. "The Costs of Foodborne Illness, Product Recalls Make the Case

for Food Safety Investments." *FoodSafety*, 2018. https://www.foodsafetymagazine.com/magazine-archive1/junejuly-2018/the-costs-of-foodborne-illness-product-recalls-make-the-case-for-food-safety-investments/.

Stoyanov, Plamen G., and Craig A. Grimes. 2000. "Remote Query Magnetostrictive Viscosity Sensor." *Sensors and Actuators, A: Physical* 80 (1): 8–14. https://doi.org/10.1016/S0924-4247(99)00288-5.

Taylor, Allen D., Jon Ladd, Qiuming Yu, Shengfu Chen, Jiří Homola, and Shaoyi Jiang. 2006. "Quantitative and Simultaneous Detection of Four Foodborne Bacterial Pathogens with a Multi-Channel SPR Sensor." *Biosensors and Bioelectronics* 22 (5): 752–58. https://doi.org/10.1016/j.bios.2006.03.012.

Vahid Rastegar, Goodarz Ahmadi, S.V. Babu, et al. 2017. "Filtration of Aqueous Colloidal Ceria Slurries Using Fibrous Filters – An Experimental and Simulation Study." *Separation and Purification Technology* 176: 231–42. https://doi.org/10.1016/j.seppur.2016.12.017.

Velusamy, Vijayalakshmi, Khalil Arshak, Olga Korostynska, Kamila Oliwa, and Catherine Adley. 2010. "An Overview of Foodborne Pathogen Detection: In the Perspective of Biosensors." *Biotechnology Advances* 28 (2): 232–54. https://doi.org/10.1016/j.biotechadv.2009.12.004.

Wan, Jiehui, Michael L. Johnson, Rajesh Guntupalli, Valery A. Petrenko, and Bryan A. Chin. 2007. "Detection of Bacillus Anthracis Spores in Liquid Using Phage-Based Magnetoelastic Micro-Resonators." *Sensors and Actuators, B: Chemical* 127 (2): 559–66. https://doi.org/10.1016/j.snb.2007.05.017.

Wikipedia. 2020a. "Antibody." 2020. https://en.wikipedia.org/wiki/Antibody.

Wikipedia. 2020b. "Bioterrorism." 2020. https://en.wikipedia.org/wiki/Bioterrorism.

Yang, Liju, Yanbin Li, Carl L. Griffis, and Michael G. Johnson. 2004. "Interdigitated Microelectrode (IME) Impedance Sensor for the Detection of Viable Salmonella Typhimurium." *Biosensors and Bioelectronics* 19 (10): 1139–47. https://doi.org/10.1016/j.bios.2003.10.009.

Yang, Liju, Chuanmin Ruan, and Yanbin Li. 2001. "Rapid Detection of Salmonella

Typhimurium in Food Samples Using a Bienzyme Electrochemical Biosensor with Flow Injection." *Journal of Rapid Methods and Automation in Microbiology*. https://doi.org/10.1111/j.1745-4581.2001.tb00249.x.

Yaron, S., and K. R. Matthews. 2002. "A Reverse Transcriptase-Polymerase Chain Reaction Assay for Detection of Viable Escherichia Coli O157:H7: Investigation of Specific Target Genes." *Journal of Applied Microbiology* 92 (4): 633–40. https://doi.org/10.1046/j.1365-2672.2002.01563.x.

Yu, Chenxu, Joseph Irudayaraj, Chitrita Debroy, Ze'ev Schmilovtich, and Amos Mizrach. 2006. "Spectroscopic Differentiation and Quantification of Microorganisms in Apple Juice." *Journal of Food Science* 69 (7): 268–72. https://doi.org/10.1111/j.1365-2621.2004.tb13627.x.

Zeynep Altintas, et al. 2018. "A Fully Automated Microfluidic-Based Electrochemical Sensor for Real-Time Bacteria Detection.Pdf." *Biosensors and Bioelectronics* 100: 541–48.

Zhao, Jianxiu, Sabrina S. Jedlicka, Josh D. Lannu, Arun K. Bhunia, and Jenna L. Rickus. 2006. "Liposome-Doped Nanocomposites as Artificial-Cell-Based Biosensors: Detection of Listeriolysin O." *Biotechnology Progress* 22 (1): 32–37. https://doi.org/10.1021/bp050154o.